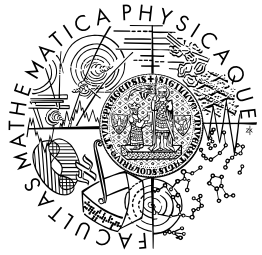

FACULTY
OF MATHEMATICS
AND PHYSICS
Charles University

BACHELOR THESIS

Jáchym Ševčík

Validation of snow cover forecast by numerical weather prediction model ALADIN

Department of Atmospheric Physics

Supervisor of the bachelor thesis: doc. Mgr. Žák Michal, Ph.D.

Study programme: Physics

Study branch: Physics

Prague 2023

I declare that I carried out this bachelor thesis independently, and only with the cited sources, literature and other professional sources. It has not been used to obtain another or the same degree.

I understand that my work relates to the rights and obligations under the Act No. 121/2000 Sb., the Copyright Act, as amended, in particular the fact that the Charles University has the right to conclude a license agreement on the use of this work as a school work pursuant to Section 60 subsection 1 of the Copyright Act.

In ..... date ....

Author's signature

I would like to thank the supervisor of this bachelor thesis, doc. Mgr. Michal Žák, Ph.D., for the assignment and for facilitating communication between me and the Czech Hydrometeorological Institute. I am thankful to RNDr. Radmila Brožková, CSc. for allowing me to carry out this thesis at the Czech Hydrometeorological Institute and for much advice and inspiring remarks. I would also like to thank Mgr. Ján Mašek, PhD, for patient explanation of topics related to the model's physics, statistical analysis and results interpretation. I am grateful to Mgr. Alena Trojáková for needed help with the problematics of the station network and script creation. Last but not least, I would like to thank my family and friends for their ongoing support of my studies.

Title: Validation of snow cover forecast by numerical weather prediction model ALADIN

Author: Jáchym Ševčík

Department: Department of Atmospheric Physics

Supervisor: Mgr. Žák Michal, Ph.D., Department of Atmospheric Physics

Abstract: This thesis deals with forecast of snow cover made by the numerical weather prediction model ALADIN and with snow cover measurements. First, it describes the model parametrization of snow-related variables. This is followed by a description of the meteorological stations network and of the snow measurements methodology. The main focus of the thesis lies on the validation of snow depth and snow water equivalent forecasts. This is done by comparison of measurements from the winter season 2021/2022 against corresponding ALADIN forecasts with forecast ranges of 6 and 30 hours. The comparison is first made with regard to the overall tendency and the magnitude of the model error. Secondly, it deals with model frequency of snow cover misses or false alarms. Finally, the thesis touches upon the validation of snow density forecast.

Keywords: snow cover forecast - validation - snow depth - snow water equivalent - density of snow

Contents

Introduction **2**

1 Parametrization of ALADIN snow cover evolution **3**
1.1 Theoretical description . . . 3
1.1.1 Snow reservoir . . . 3
1.1.2 Snow albedo . . . 4
1.1.3 Snow density . . . 5
1.1.4 Snow depth . . . 6
1.1.5 Snow fraction . . . 6

2 Snowpack measurements **8**
2.1 Station network in Czechia . . . 8
2.2 Snow depth measurements . . . 8
2.3 Snow water equivalent measurements . . . 9

3 ALADIN forecast validation **10**
3.1 Used statistical measures . . . 10
3.2 Snow depth validation . . . 11
3.2.1 Snow depth station analysis . . . 11
3.2.2 Comparison of observed and forecast snow depth . . . 14
3.3 Snow water equivalent validation . . . 23
3.3.1 Snow water equivalent station analysis . . . 23
3.3.2 Comparison of observed and forecast snow water equivalent 24
3.4 Snow density validation . . . 35

Conclusion **37**

Bibliography **38**

List of Figures **40**

List of Tables **43**

List of Abbreviations **44**

A Attachments **45**
A.1 Code implementation . . . 45
A.1.1 Snow tendencies . . . 45
A.1.2 Snow variables evolution . . . 45
A.1.3 Snow fractions . . . 46

Introduction

Snow cover is an important component of the global climate system. Fresh snow has high values of reflectivity, increasing the surface albedo. High thermal emissivity of snow influences the amount of energy lost by infrared radiation. Its low thermal conductivity causes it to partly insulate the ground from the atmosphere. The snowpack is an important reservoir of water, that is released during spring melting. At this period, high value of snow specific latent heat prevents the rise of underlying surface temperature. Its occurrence can also significantly lower surface roughness, affecting the height of the friction layer. Through these characteristics, snow affects the radiation, thermal and hydrological balance of the Earth's surface as well as its mechanical properties.

The above-mentioned impacts make it important for numerical weather prediction models to accurately parametrize the evolution and properties of snow, especially in regions with variable snow cover, such as Czechia.

To have a well-calibrated snow scheme, it is first necessary to know its current accuracy and systematic behaviour. This is the main aim of the thesis, which focuses on the ALADIN model and the validation of its snow cover forecast. The thesis is divided into three main sections. The first section briefly presents the ALADIN model and its snow parametrization. The second section introduces the station network used for snow observations and summarizes the methodology of snow measurements. The third section compares measured and forecast data from the winter season 2021/2022. This comparison is separated into three subsections. They deal with the validation of snow depth, snow water equivalent, and snow density. Finally, the results are summarized, and a possible cause for the model error is outlined in the conclusion. The more technical part of the text dealing with code implementation of the relations from the first section is in the attachments chapter.

1. Parametrization of ALADIN snow cover evolution

1.1 Theoretical description

ALADIN[1] is a numerical weather prediction system which originated as a limited-area version of the global ARPEGE[2] model established by Météo-France. It is being developed by a consortium of 16 European and northern African countries, which are also using it for their weather-forecasting applications (Termonia et al. [2018]).

At the Czech HydroMeteorlogical Institute, one of ALADIN so-called canonical configurations ALARO[3] is being developed and used, with its current resolution of $2,325\,\mathrm{km}$ (Brožková et al. [2019]).

Two different approaches to snow parametrization can be used in the soil-vegetation scheme of the model, one being the Douville et al. [1995] scheme and the second one the Bazile et al. [2001] scheme. In the model code these schemes are implemented respectively under keys `LSNV` and `LVGSN`. Since the current version of the model snow treatment used at CHMI is based on the latter, that one will be described in more detail. A schematic view of different reservoirs and water transfers in the ISBA[4] scheme is shown in Fig. 1.1. ISBA is part of the model code dealing with soil variables, including the ones regarding snow.

In this scheme, the snowpack is characterized by 3 prognostic variables: snow water equivalent alias snow reservoir, albedo and density. The model calculates the value of these variables from their time evolution $\frac{\partial X_\mathrm{s}}{\partial t}$ in the following way

$$X_\mathrm{s}(t+\Delta t) = X_\mathrm{s}(t) + \Delta t \cdot \frac{\partial X_\mathrm{s}}{\partial t}(t), \tag{1.1}$$

where X_s stands for any of the 3 mentioned prognostic variables and Δt is the time step of model integration. It is thus an explicit time marching scheme, where right-hand side terms are evaluated at time level t. Time evolution of prognostic variables is described in subsections 1.1.1 - 1.1.3. Additional characteristics - snow depth and snow fraction - are diagnosed accordingly to subsections 1.1.4 and 1.1.5.

1.1.1 Snow reservoir

Snow reservoir is in this case represented by snow water equivalent W_s $[\mathrm{kg\,m^{-2}}]$. W_s is the amount of water contained in snowpack per unit area. Its evolution is, according to Gerard [2005], described by equation

$$\frac{\partial W_\mathrm{s}}{\partial t} = \mathcal{P}_\mathrm{s} - F_\mathrm{m} + (F_\mathrm{evs} - F_\mathrm{evi}), \tag{1.2}$$

[1] Aire Limitée Adaptation Dynamique développement InterNational

[2] Action de Recherche Petite Echelle Grande Echelle

[3] Short for ALadin–AROme, where AROME stands for Application of Research to Operations at Mesoscale

[4] Interactions Sol Biosphère Atmosphère

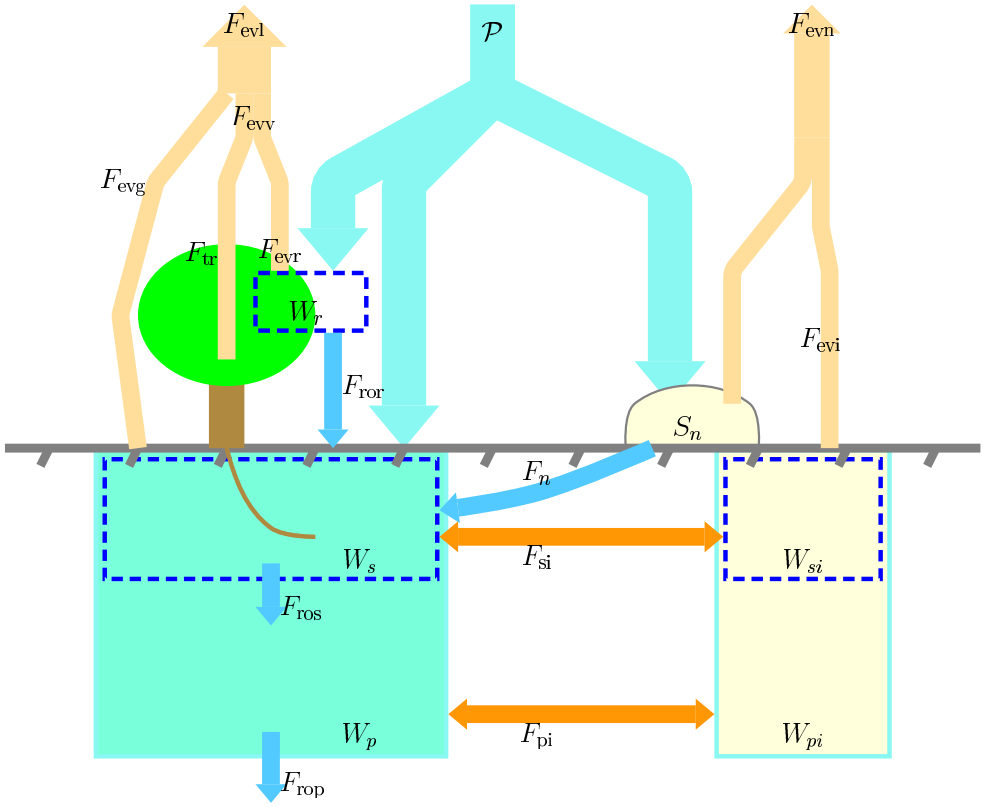

Figure 1.1: Schematic view describing various reservoirs and fluxes in the ISBA scheme, an image courtesy of Luc Gerard (Gerard [2005]). Notation in the scheme is derived from French. However, further in the text, these English-derived equivalents will be used: snow reservoir $S_{\mathrm{n}} \to W_{\mathrm{s}}$, snow melting flux $F_{\mathrm{n}} \to F_{\mathrm{m}}$, flux from solid reservoirs $F_{\mathrm{evn}} \to F_{\mathrm{evs}}$

where $\mathcal{P}_{\mathrm{s}}$ is the flux of solid precipitation, F_{m} is the snow melting flux and $(F_{\mathrm{evs}} - F_{\mathrm{evi}})$ is the evaporation flux from snow reservoir, given as the difference of evaporation flux from solid reservoirs (snow plus ice) and the evaporation flux from the ice reservoir alone. The plus sign preceding $F_{\mathrm{evs}} - F_{\mathrm{evi}}$ is consistent with a convention that the value of vertical fluxes is negative in the upward direction. In the case of horizontal snow melting flux F_{m}, the value is positive when melting occurs and therefore its sign in snow reservoir evolution has to be negative. The unit of all mentioned fluxes is $[\mathrm{kg\,m^{-2}\,s^{-1}}]$.

The value of snow reservoir computed from its time tendency according to Eq. (1.1) has to be non-negative. That is secured by the truncation

$$W_{\mathrm{s}} := \max(0, W_{\mathrm{s}}(t)), \tag{1.3}$$

where $:=$ denotes assignment in the model code.

1.1.2 Snow albedo

Time evolution of snow albedo $A_{\mathrm{n}} \to A_{\mathrm{s}}$, is evaluated at time level t according to the following equation (Gerard [2005]):

$$\frac{\partial A_{\mathrm{s}}}{\partial t} = \frac{\mathcal{P}_{\mathrm{s}}}{W_{\mathrm{s}}^{\mathrm{new}}} - \begin{cases} r_{\mathrm{exp}}(A_{\mathrm{s}} - A_{\mathrm{s}}^{\mathrm{min}}) & \text{if } F_{\mathrm{m}} > 0 \\ r_{\mathrm{lin}} & \text{if } F_{\mathrm{m}} \leq 0, \end{cases} \tag{1.4}$$

where $W_{\mathrm{s}}^{\mathrm{new}}$ is the minimum amount of snowfall necessary to renew snow albedo, $A_{\mathrm{s}}^{\mathrm{min}}$ is minimum snow albedo, r_{exp} denotes the exponential decrease rate in snow albedo and snow density during snow melting, while r_{lin} is the linear decrease rate in snow albedo in freezing conditions.

The actual value of snow albedo is again given by Eq. (1.1) and it is secured from overflowing into non-physical values by truncation

$$A_{\mathrm{s}} \coloneqq \min\Big(\max(A_{\mathrm{s}}, A_{\mathrm{s}}^{\mathrm{min}}\Big), A_{\mathrm{s}}^{\mathrm{max}}). \tag{1.5}$$

Thanks to Eq. (1.5), snow albedo cannot take values lower than minimum snow albedo $A_{\mathrm{s}}^{\mathrm{min}}$ and higher than maximum snow albedo $A_{\mathrm{s}}^{\mathrm{max}}$.

The final gridbox albedo is then, according to Bazile et al. [2001], estimated as

$$A = (1 - f_{\mathrm{veg}}) \cdot \Big(A_{\mathrm{bg}} \cdot (1 - f_s^{\mathrm{bg}}) + A_{\mathrm{s}} \cdot f_{\mathrm{s}}^{\mathrm{bg}}\Big) + f_{\mathrm{veg}} \cdot \Big(A_{\mathrm{veg}} \cdot (1 - f_{\mathrm{s}}^{\mathrm{veg}}) + A_{\mathrm{s}} \cdot f_{\mathrm{s}}^{\mathrm{veg}}\Big),$$

where A_{bg} is the albedo of snow-free bare ground and A_{veg} the albedo of snow-free vegetation, f_{veg} is fraction of vegetation, $f_{\mathrm{s}}^{\mathrm{bg}}$ is fraction of snow on bare ground, and $f_{\mathrm{s}}^{\mathrm{veg}}$ is fraction of snow on vegetation.

1.1.3 Snow density

According to Gerard [2005], the evolution of snow density ρ_{s} evaluated at time level t is treated as follows:

$$\frac{\partial \rho_{\mathrm{s}}}{\partial t} = -r_{\mathrm{exp}}(\rho_{\mathrm{s}} - \rho_{\mathrm{s}}^{\mathrm{max}}) - \min\left(\frac{\mathcal{P}_{\mathrm{s}}}{\max(W_{\mathrm{s}}, \epsilon)}, \frac{1}{2\Delta t}\right)(\rho_{\mathrm{s}} - \rho_{\mathrm{s}}^{\mathrm{min}}). \tag{1.6}$$

Here $\rho_{\mathrm{s}}^{\mathrm{min}}$ and $\rho_{\mathrm{s}}^{\mathrm{max}}$ denote minimum and maximum snow densities. The first term on the right-hand side of this equation has a positive value and represents growth in density caused by the settling of snowpack over time. The second term ensures a decrease in density of snowpack in case of snowfall. It is supposed that fresh snow has minimum density $\rho_{\mathrm{s}}^{\mathrm{min}}$. The denominator $\max(W_{\mathrm{s}}, \epsilon)$ then ensures that the whole fraction $\mathcal{P}_{\mathrm{s}}/\max(W_{\mathrm{s}}, \epsilon)$ does not approach infinity in case of snowfall onto snow-free ground. The purpose of the above minimum function, limiting the rate of change towards $\rho_{\mathrm{s}}^{\mathrm{min}}$, can be best viewed by omitting the settling term and supposing heavy snowfall with $(\mathcal{P}_{\mathrm{s}}/\max(W_{\mathrm{s}}, \epsilon)) \geq (1/2\Delta t)$. Then, breaking down the derivative and the expression containing model time step Δt in a discretized form, yields:

$$\frac{\rho_{\mathrm{s}}(t + \Delta t) - \rho_{\mathrm{s}}(t)}{\Delta t} = -\frac{1}{2\Delta t}(\rho_{\mathrm{s}}(t) - \rho_{\mathrm{s}}^{\mathrm{min}})$$

By simple manipulations we obtain

$$\rho_{\mathrm{s}}(t + \Delta t) = \frac{\rho_{\mathrm{s}}(t) + \rho_{\mathrm{s}}^{\mathrm{min}}}{2}. \tag{1.7}$$

From Eq. (1.7) it is apparent that the minimum function in Eq. (1.6) prevents snow density from decreasing too fast in case of heavy snowfall, by allowing the value of $\rho_{\mathrm{s}}(t + \Delta t)$ to only decrease half-way to the value of $\rho_{\mathrm{s}}^{\mathrm{min}}$ in one time step. That is a simple way of taking into account higher density of snowpack, onto which fresh snow is falling.

Analogously to snow reservoir and albedo, the actual value of snow density can be obtained from Eq. (1.1). The physical limits of ρ_{s} are secured by truncation

$$\rho_{\mathrm{s}} \coloneqq \min\Big(\max(\rho_{\mathrm{s}}, \rho_{\mathrm{s}}^{\mathrm{min}}\Big), \rho_{\mathrm{s}}^{\mathrm{max}}). \tag{1.8}$$

1.1.4 Snow depth

Snow depth d_s [m] can be diagnosed from snow reservoir W_s and snow density ρ_s using the relation

$$d_\mathrm{s} = \frac{W_\mathrm{s}}{\rho_\mathrm{s}}. \tag{1.9}$$

W_s is snow mass m_s per unit area and ρ_s is snow mass m_s per unit volume as is depicted in Fig. 1.2.

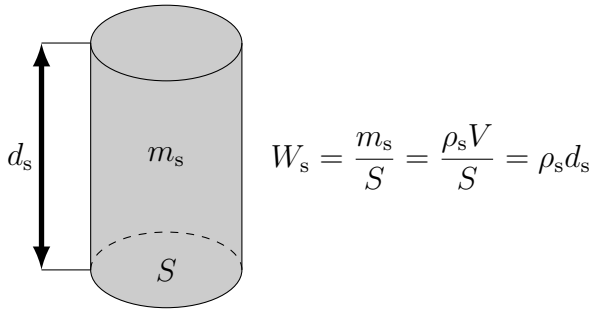

Figure 1.2: A diagram illustrating the relationship between snow depth and snow reservoir

1.1.5 Snow fraction

Snow fraction f_s represents the share of the gridbox surface, which is effectively covered by snow. According to Mašek [2018] the following sum for computing total gridbox snow fraction is currently being used

$$f_\mathrm{s} = (1 - f_\mathrm{veg}) f_\mathrm{s}^\mathrm{bg} + f_\mathrm{veg} f_\mathrm{s}^\mathrm{veg},$$

f_veg being the vegetation fraction. The snow fraction over bare ground f_s^bg is diagnosed by a hyperbolic formula

$$f_\mathrm{s}^\mathrm{bg} = \frac{W_\mathrm{s}}{W_\mathrm{s} + W_\mathrm{s}^\mathrm{crit}\left(1 + \frac{z_\mathrm{0D}^\mathrm{bg}}{a_2}\right)}, \tag{1.10}$$

where W_s represents the snow reservoir and $W_\mathrm{s}^\mathrm{crit}$ is a constant critical value of it. The bracket in the denominator lowers the value of f_s^bg, taking into account the effect of surface roughness. Here z_{0D}^bg represents dynamic roughness length of bare ground and a_2 is a tuning parameter. Dynamic roughness length z_0D is the height at which the logarithmic profile of wind, extrapolated from the inertial layer, goes to zero (Bednář and Zikmunda [1985]). Typically it equals to $\frac{1}{10}$ of the height of roughness elements. The value of $z_\mathrm{0D}^\mathrm{bg}$ does not exceed 2 m and a_2 is set to 10 m, therefore the effect of surface roughness can only cause a rather small increase of the value of $W_\mathrm{s}^\mathrm{crit}$ by a factor of 1.2 (Mašek [2018]).

The snow fraction over vegetation $f_\mathrm{s}^\mathrm{veg}$ is given by

$$f_\mathrm{s}^\mathrm{veg} = F(\mathrm{LAI}, A_\mathrm{s}) f_\mathrm{s}^\mathrm{bg},$$

where $F(\mathrm{LAI}, A_\mathrm{s})$ is a factor depending on snow albedo A_s and the Leaf Area Index LAI so that

$$F(\mathrm{LAI}, A_\mathrm{s}) = \begin{cases} 1 & \text{if } LAI < 3 \\ 1 - \min\left(1, \dfrac{LAI}{K_\mathrm{lai}}\right) \cdot \dfrac{A_1 - max(A_2, A_\mathrm{s})}{A_1 - A_2} < 1 & \text{if } LAI \geq 3, \end{cases} \tag{1.11}$$

where K_lai, A_1 and A_2 are tuning parameters. This configuration reflects on the fact, that fresh snow can stick to high vegetation and fall down as it becomes older. For low vegetation, this effect is much less pronounced (Bazile et al. [2001]).

2. Snowpack measurements

According to Lipina et al. [2022], snow cover is considered to be a layer of snow or ice, which has occurred as a consequence of solid precipitation such as snow, hailstones, snow pellets, snow grains, ice pellets, small hail or ground ice. At CHMI stations, the following characteristics of snow are being measured:

- snow depth d_s,
- snow water equivalent W_s,
- fresh snow depth.

In the case of this thesis, only data from snow depth and snow water equivalent measurements have been used. These are both being measured only in case of continuous snow cover, which stands for snowpack covering more than half of the station's area and its surroundings (Lipina et al. [2022]).

2.1 Station network in Czechia

For this validation, measurement data from the CHMI climatological database CLIDATA were used. This database gathers measurements from various types of stations. These stations can be classified based on different criteria, for instance, one can distinguish professional and volunteer meteorological stations (Lipina et al. [2021]). Professional stations can be then divided into groups based on their observation program, while volunteer stations are usually sorted with regard to their equipment, way of data entry and presence of an observer.

Apart from professional and volunteer meteorological stations, the database also collects data from a wide range of other station types, often referred to as additional. Data from these stations are not being systematically checked and their sensors are not regularly calibrated by CHMI. Among these stations are for example CHMI hydrological stations, which provide data about water level, water temperature and runoff. They also include automatic snow-measuring devices, also called snow pillows. As additional are also considered weekly snow profile measurements, stations owned by non-professional meteorologists and organizations, hydrological stations owned by the Czech Water Management Enterprises and other waterworks companies which provide their data to CHMI and finally, manual stations which serve for checking automatic precipitation- and snow-measuring stations (Lipina et al. [2021]).

Data from all of these mentioned types of stations were contained in a primary selection made for this validation, which has been later narrowed down, as is described further in the text.

2.2 Snow depth measurements

Snow depth is measured by manual and automatic stations. Manual stations measure snow daily at 06 UTC, automatic stations every 10 minutes. In the case of manually operated stations, a snow stake is being used, while automatic

stations have laser and ultrasonic sensors at their disposal. The measurement should be made in a place unaffected by wind. At stations with exceptionally deep snow, 2 to 3 m long stakes are being used, at regular stations 1 m stakes are enough. In specific situations, these symbols are being used for the record:

- 0N - not continuous snow cover
- 0P - "trace"
- 0A - anthropogenic influence

As "trace" is referred to snow cover of fewer than 0.5 cm. However, in the case of the data used for this validation, all measured values have been rounded to whole centimetres (Lipina et al. [2022]). This means that snow "trace", as well as all the other specific situations, was equivalent to no snow cover at all.

2.3 Snow water equivalent measurements

Snow water equivalent is being measured weekly, every Monday at 06 UTC in the proximity of the place of snow depth measurement. At regular weather stations, solid precipitation is collected using a snow gauge, in which it is subsequently melted and the height of the water column is measured (Lipina et al. [2022]). In the case of automatic stations, the value of W_s is obtained by weighing on a snow pillow. Snow pillow is an automatic measuring device which, among other meteorological elements, estimates the value of snow water equivalent, using hydrostatic pressure inside a bag filled with an antifreeze liquid or by weighing snowpack on tenzometric scales (Česká meteorologická společnost).

At regular climatological stations with an observer, W_s is measured only in case of snow cover deeper than 4 cm. At professional stations, this threshold is lowered to 1 cm and on the specific stations used for hydrological forecast, snow water equivalent is being measured for snow depth greater than 0.5 cm. In all cases, the value is rounded to a tenth of a mm of the water column height. Alternatively, $\mathrm{kg\,m^{-2}}$ can be used, as the height of a water column from 1 kg of water on an area of $1\,\mathrm{m^2}$ is 1 mm. By that is assumed that water density is $1000\,\mathrm{kg\,m^{-3}}$, which is an approximation commonly used in practice.

3. ALADIN forecast validation

3.1 Used statistical measures

For comparison of observed and forecast data, these three statistical measures have been used: bias b, standard deviation σ and root mean square error δ. For clarity, one can define the forecast error vector as

$$\boldsymbol{E} = \boldsymbol{X}^{\mathrm{f}} - \boldsymbol{X}^{\mathrm{o}},$$

where $\boldsymbol{X}^{\mathrm{o}}$ is a vector consisting of observed values for different stations and the elements of $\boldsymbol{X}^{\mathrm{f}}$ are the forecast values for the model grid points in the closest proximity of the respective stations. Since bias is the average error of the forecast (Coiffier [2011]), it is given by

$$b = \frac{1}{N}\sum_{i=1}^{N} E_i, \tag{3.1}$$

where N is the number of measuring stations. Bias b then expresses the systematical component of forecast error.

Analogously to absolute bias, relative bias $b^{(\mathrm{r})}$ is defined as

$$b^{(\mathrm{r})} = \frac{\sum_{i=1}^{N}(X_i^{\mathrm{f}} - X_i^{\mathrm{o}})}{\sum_{i=1}^{N} X_i^{\mathrm{o}}}. \tag{3.2}$$

Relative bias serves as a useful measure for comparing systematic error of forecast between different station groups or quantities.

The standard deviation σ can be interpreted as an indicator of the variability or spread around the bias values in the data set. It is defined as

$$\sigma = \sqrt{\frac{1}{N}\sum_{i=1}^{N}(E_i - b)^2}, \tag{3.3}$$

and root mean square error is defined as

$$\delta = \sqrt{\frac{1}{N}\sum_{i=1}^{N} E_i^2}. \tag{3.4}$$

It can also be shown that these three measures are connected by a simple relation (Coiffier [2011])

$$\delta^2 = b^2 + \sigma^2. \tag{3.5}$$

The averaging in Equations (3.1), (3.2), (3.3) and (3.4) was done over all the stations available on a specific day. By applying them daily in case of snow depth or weekly in case of snow water equivalent, one can obtain these characteristics in the form of a time series. To get the total value of these statistical measures over the whole season, they can be averaged as follows: The value of total bias B is given by the weighted average

$$B = \frac{\sum_{j=1}^{M} N_j b_j}{\sum_{j=1}^{M} N_j},$$

where M is the number of time slots or days on which measuring was carried out, $\boldsymbol{N}$ is a vector of daily station counts, and $\boldsymbol{b}$ is a vector of daily biases computed according to Eq. (3.1).

In the case of total relative bias, another form of weighed average has to be used:

$$B^{(\mathrm{r})} = \frac{\sum_{j=1}^{M} X_j^{\mathrm{o}} b_j^{(\mathrm{r})}}{\sum_{j=1}^{M} X_j^{\mathrm{o}}}.$$

Here the weights $X_j^o = \sum_{i=1}^{N_j} X_{ij}^o$ are daily sums of observed values. Days on which X_j^o was equal to 0 and $b^{(\mathrm{r})}$ was thus not defined were simply left out from the calculation $B^{(\mathrm{r})}$.

Due to the properties of square root, the value of total root mean square error Δ has to be calculated as

$$\Delta^2 = \frac{\sum_{j=1}^{M} N_j (\delta_j)^2}{\sum_{j=1}^{M} N_j},$$

where $\boldsymbol{\delta}$ stands for the vector of daily values of root mean square errors given by Eq. (3.4).

Finally, since Eq. (3.5) holds universally, the value of standard deviation over whole season Σ can be determined from

$$\Sigma^2 = \Delta^2 - B^2. \tag{3.6}$$

3.2 Snow depth validation

3.2.1 Snow depth station analysis

The period of this validation is the winter season 2021/2022, specifically from 1st November 2021 to 2nd May 2022. In the case of snow depth, data with daily measurements from 436 stations were available. These were picked from all available stations measuring snow depth, based on their reliability by CHMI experts (A. Trojáková, personal communication, January 2023). However, not all these stations have measured on each day, leading to problematic behaviour of average snow depth time series. This can be well illustrated by the case of a group of 19 stations with altitudes greater than 800 m a.s.l., which provided measurements only on Mondays. Since the value of snow depth measured by these stations was substantially higher than the average, they have caused periodically recurring peaks in the time series. For these reasons, only data from stations which have measured regularly every day were used in the case of snow depth, reducing the total number of available stations to 366. These stations were then sorted based on their altitude into 4 categories. These groups are summarized, together with the area of Czechia covered by them, in Tab. 3.1 (P. Lipina, personal communication, April 2023).

The spatial distribution of these 4 groups and the excluded stations is displayed in Fig. 3.1. Counts of all and regularly measuring stations are summarized in Tab 3.2.

The loss of data caused by omitting irregularly measuring stations is the most significant for mountain stations. In their case, the 19 above-mentioned problematic stations make up approximately 35.2 % of the total amount of mountain

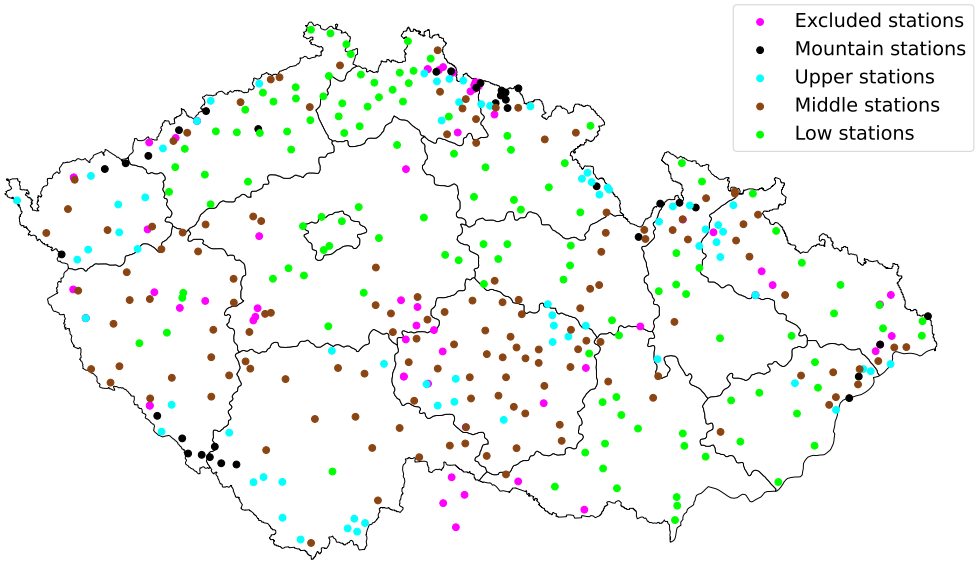

Figure 3.1: Map of excluded and used snow-depth-measuring stations distinguishing 4 altitude categories

Table 3.1: Altitude limits of the 4 categories and percentage of Czechia's area covered by them

	mountain	upper	middle	low
altitude [m a.s.l.]	> 800	$600 - 800$	$400 - 600$	< 400
area [%]	4.2	12.4	41.7	41.7

Table 3.2: Counts of stations which measured snow depth at least once, counts of regularly measuring stations and their percentage of the original count

	total	mountain	upper	middle	low
all stations	436	54	83	166	133
regularly measuring	366	35	70	139	122
percentage [%]	83.9	64.8	84.3	83.7	91.7

stations. Thanks to consultations with CHMI experts, it was found that data from these stations originate from weekly profile observations. Profile observations are the result of 10 measurements of snow depth, which are being averaged and can be therefore considered more accurate than ordinary observations.

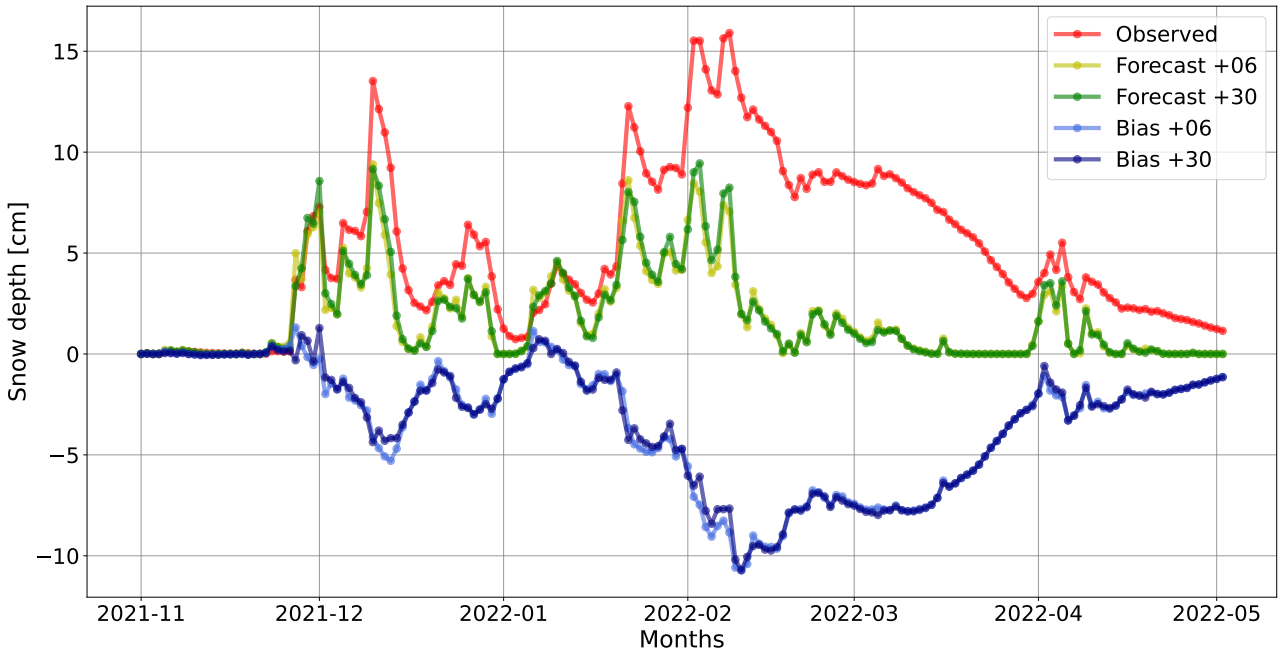

Figure 3.2: Daily time series of observed and forecast snow depth, averaged over all regularly measuring stations and their absolute bias, at forecast ranges 6 and 30 hours

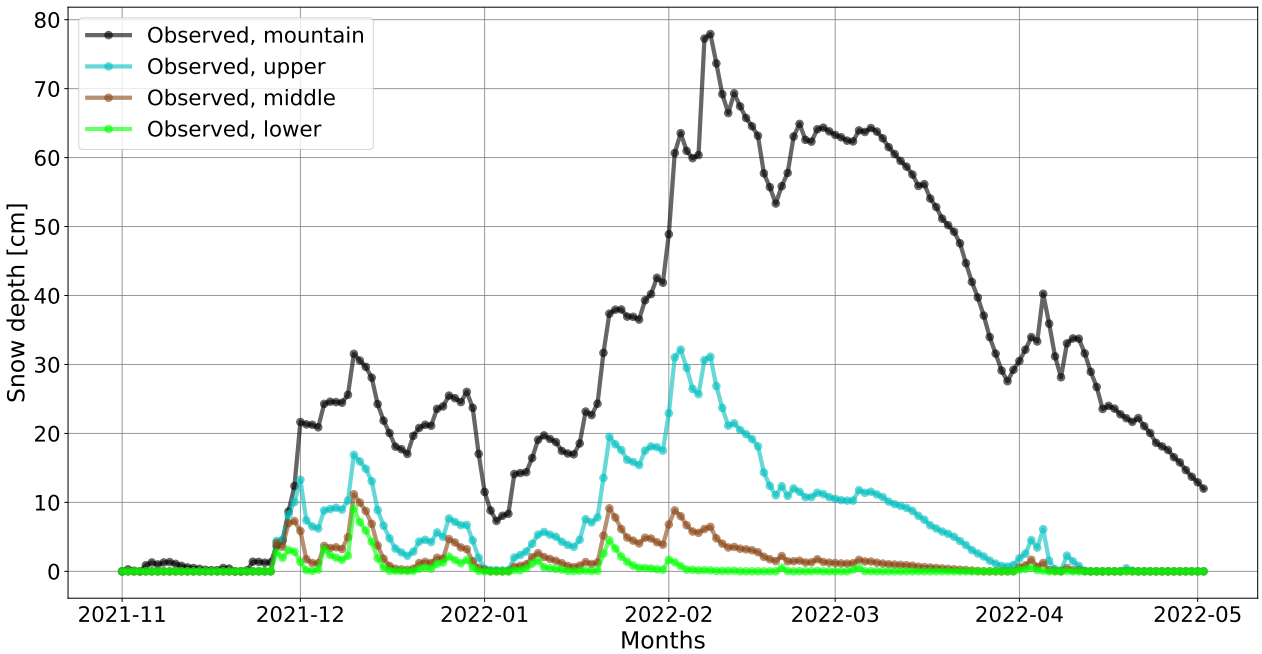

Figure 3.3: Daily time series of observed snow depth averaged over different altitude groups

Since all these problematic mountain stations have provided Monday measurements with relative availability $> 85\,\%$, a separate Monday time series could have been made for them, to avoid losing data from this amount of mountain stations. By relative availability is meant the ratio of the number of measurements made by a station and the maximum number of measurements possible. This approach, which allows the number of stations to vary over the course of time, could potentially cause some inaccuracy. Nonetheless, it has been chosen, since the main objective of this work is not to look into the time evolution of snowpack but to compare the observed and forecast values.

3.2.2 Comparison of observed and forecast snow depth

Observed data have been compared to daily forecasts of snow depth with forecast ranges of 6 and 30 hours. These data have been taken from the archive of CHMI, and since the software for forecast validation commonly used at CHMI does not support snow-related variables, the data have been processed using a tool developed for this work, based on Python. Additionally, snow depth is not a model prognostic variable and had to be estimated from forecast snow water equivalent W_s and density ρ_s using Eq. (1.9).

Comparing the forecast and observations averaged over all stations, the model turned out to underestimate the value of snow depth. The total value of bias is approximately $-3.4\,\mathrm{cm}$ in the case of the 6 hour forecast range and $-3.3\,\mathrm{cm}$ for the 30 hour one. From these values and also from Fig. 3.2, it can be seen that the difference between both forecast ranges is not very significant.

From Fig. 3.2 it is also evident that the model seems to have a tendency to underestimate the snow accumulation phase while exaggerating the melting phase. This tendency is most pronounced during February and March with the greatest forecast error occurring on February 10, when bias of the 6-hour forecast was at its minimum value of $-10.71\,\mathrm{cm}$.

However, as can be seen from Fig. 3.3, there are significant differences in observed snow depth among the mentioned altitude groups and one can expect the forecast error to vary with altitude as well. A very rough idea about the dependence of model error on altitude can be obtained from Fig. 3.4. Even though these graphs do not provide much information about the frequency of under- or overestimation due to high density of the scattered points, they show that in the case of middle, upper and especially mountain stations, the values of model error are generally greater when the forecast is underestimated. For instance, in the case of mountain stations, complete misses of values up to $1.5\,\mathrm{m}$ can be seen. On the other hand, for lower altitudes the distribution seems to be rather symmetrical, suggesting that there is not a prevalent tendency of systematic error.

These conclusions are consistent with the time series and statistical scores of the altitude groups evaluated separately. The averages of bias B and the other statistical measures for all groups are summarized in Tab. 3.3 and Tab. 3.4. Looking at them, it is obvious that from the perspective of root mean square error, integrating both bias and standard deviation, the $30\,\mathrm{h}$ forecast range performs slightly better for most of the altitude groups. On the other hand, the order of magnitude of this difference between the two forecast ranges is percent units of the actual values and can be thus considered negligible.

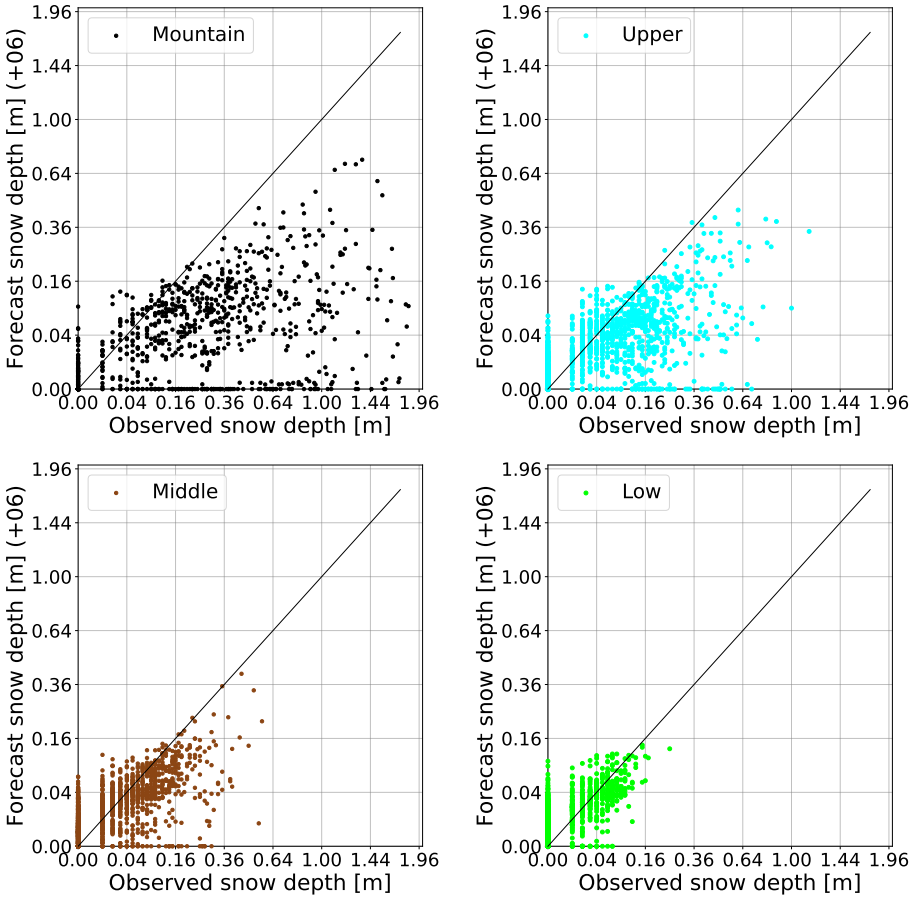

Figure 3.4: Scatter plots comparing forecast and observed snow depth for different altitude groups, both axes with square root scale, at 6 h forecast range

Table 3.3: Values of used statistical characteristics for all regularly measuring (denoted rm) stations together and split accordingly to altitude groups, values of scores of all mountain stations measuring on Mondays, at 6 h forecast range

	rm	all mnt.	rm mnt.	rm upp.	rm mid.	rm low
B [cm]	-3.4	-34.5	-24.9	-4.3	-0.6	0.1
$B^{(r)}$ [%]	-65.4	-81.5	-80.4	-60.8	-31.2	18.9
Σ [cm]	14.1	42.2	35.4	10.6	3.7	1.1
Δ [cm]	14.5	54.5	43.3	11.4	3.7	1.1

From Tab. 3.3 and Tab. 3.4 and also from the daily time series of snow depth averaged over all regularly measuring mountain stations in Fig. 3.5 can be clearly seen, that ALADIN indeed underestimates snow depth in mountain altitudes, with values of bias exceeding -0.5 m during February and March. Moreover, the inclination of bias towards negative values gets even more significant in the case of the Monday time series, which contains data from all mountain stations, including the more exact profile measurements. This time series is plotted in Fig. 3.6.

Table 3.4: The same as in Tab. (3.3) for 30 h forecast range

	rm.	all mnt.	rm mnt.	rm upp.	rm mid.	rm low
B [cm]	-3.3	-34.0	-24.4	-4.2	-0.6	0.1
$B^{(r)}$ [%]	-64.3	-80.2	-78.8	-59.5	-32.1	18.0
Σ [cm]-	13.9	41.9	35.1	10.5	3.6	1.1
Δ [cm]	14.3	54.0	42.7	11.3	3.7	1.1

Figure 3.5: Time series of daily snow depth measurements, forecasts and their absolute bias for all regularly measuring stations in mountain altitudes

From the values of seasonal bias and standard deviation (Tab. 3.3, Tab. 3.4), it can be seen that standard deviation dominates bias in the case of all altitude groups. In other words, the random component of forecast error is more significant than the systematical one. However, this is partly caused by seasonal standard deviation taking into account the interdiurnal variability, when being calculated according to Eq. (3.6). For the daily values of standard deviation σ and bias b, which can not include this information, the value of σ is being dominated by b in the case of mountain altitudes. That can be seen from Fig. (3.7), leaving space for improvement of the current forecast approach.

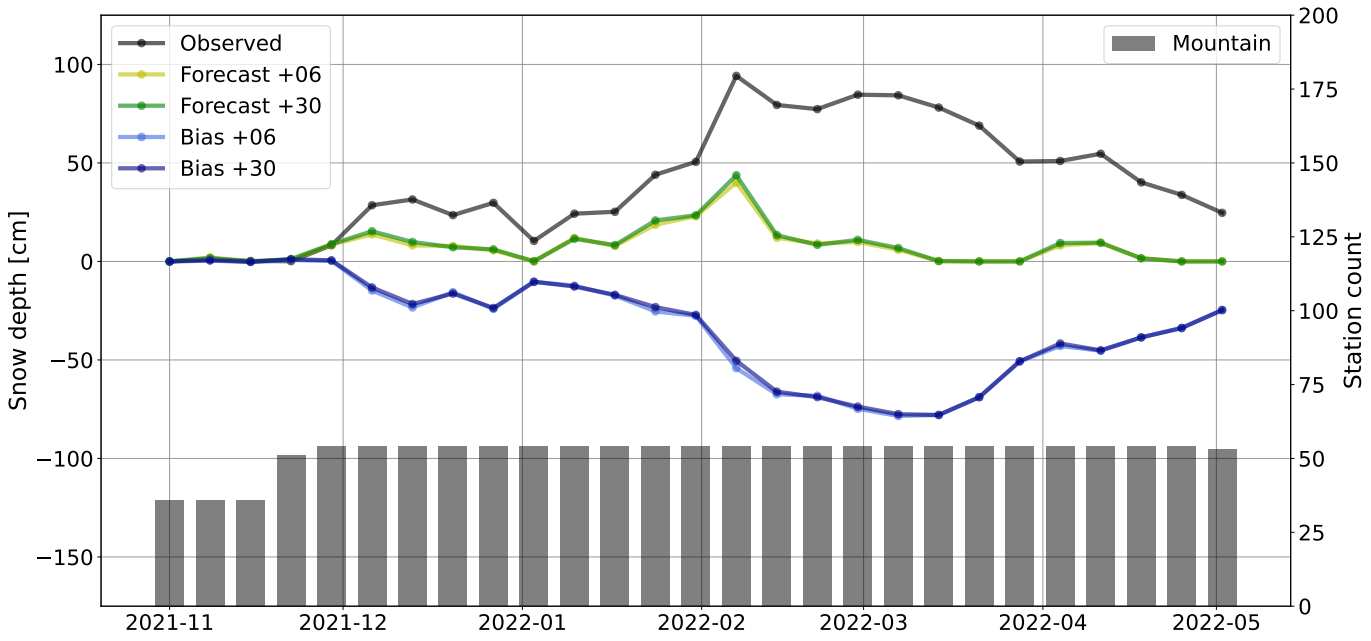

Figure 3.6: Time series of weekly snow depth measurements, forecasts and their absolute bias for all stations in mountain altitudes, barplots with counts of stations available on the day of measurement

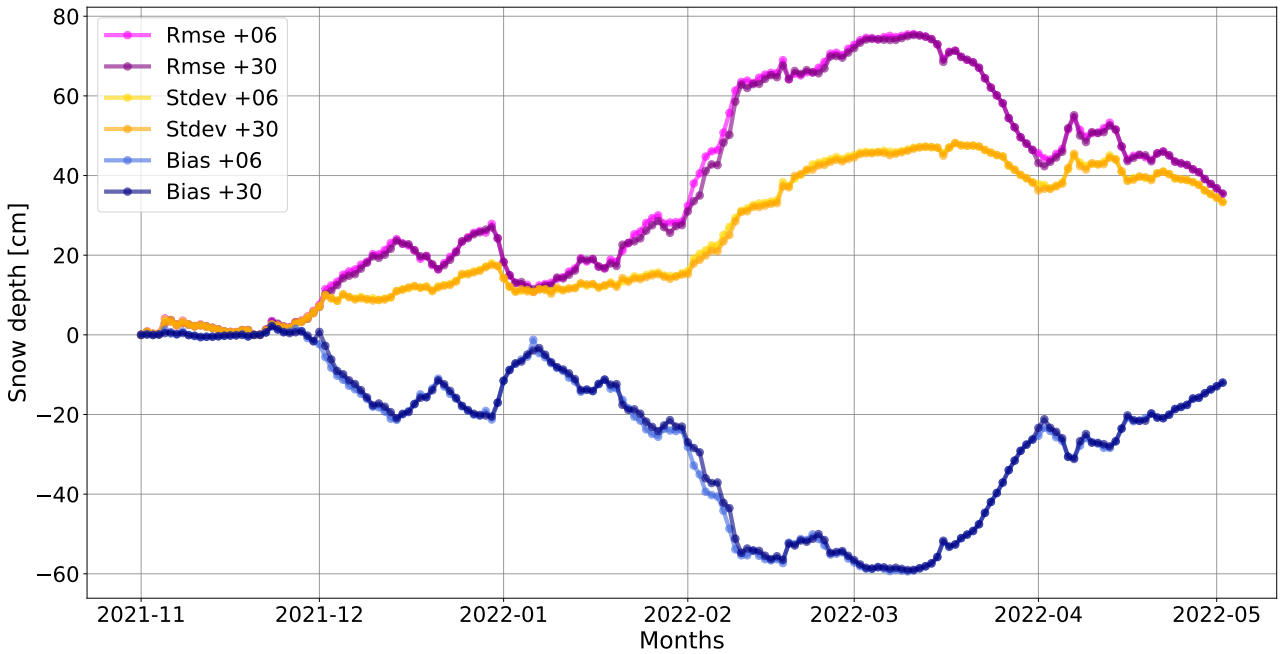

Figure 3.7: Daily time series of used statistical scores for mountain regularly measuring stations

The conclusion that forecast snow depth is being underestimated in the case of mountain altitudes is also supported by the bias frequency distribution of all regularly measuring mountain stations in Fig. 3.8. The marginal bins in this figure, and also in all the following histograms, contain values from all the bins exceeding the selected x-axis range. The mean value of this distribution is negative for the mountain stations and the 6 h forecast range. This can be seen from Tab. 3.5, which also includes mean and standard deviation of snow depth bias distributions for all the other altitude groups. The same information for the 30 h forecast range is in Tab. 3.6.

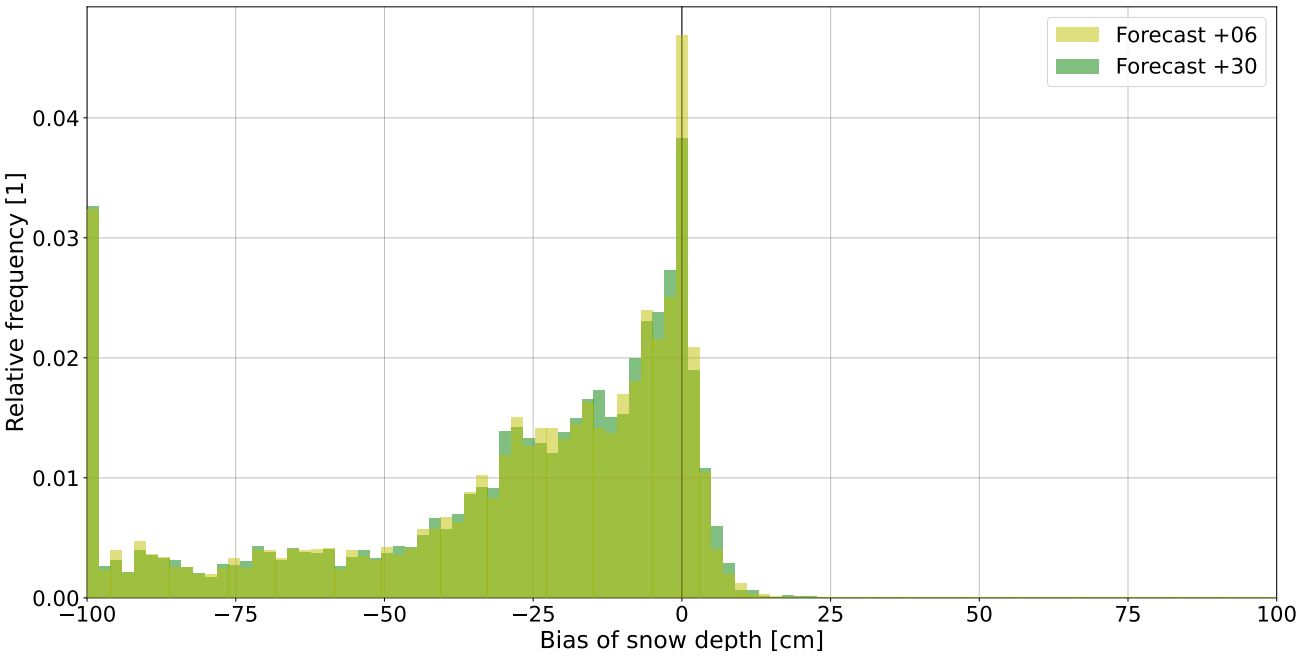

Figure 3.8: Frequency distribution of snow depth forecast bias for regularly measuring stations in mountain altitudes, at 6 h and 30 h forecast ranges

In this analysis, all the values of zero bias originating from correct forecasts of no snow cover were omitted, since they caused the histograms to have very little information value. Consequently, Fig. 3.8 and all the other histograms only provide information about the predominant tendency of forecast bias, but not about the total counts of correct and false forecasts. This adjustment of the data set also explains the change in performance difference between the two forecast ranges. From the seasonal values of bias (see Tab. 3.3, Tab. 3.4), the 30 h forecast range comes out as more accurate, while in the case of bias frequency distribution, the absolute values of mean bias are mostly smaller for the 6 h one (Tab. 3.5, Tab. 3.6). This is most likely caused by the model being slightly more accurate in forecasting no snow cover 30 hours in advance, causing it to be penalized more by the exclusion of such cases.

From all the above-mentioned tables it can be seen, that even though the tendency to underestimate snow depth gets quantitatively less significant for upper and middle stations, it is still present. However, the situation is different for lower stations. In their case, the model has a tendency to overestimate snow depth as can also be seen from Fig. 3.9 and Fig. 3.10.

Table 3.5: Mean and standard deviation of bias distributions for all altitude groups, 6 h forecast range, zero bias values originating from correct forecast of no snow omitted, (regularly measuring stations denoted as rm)

	rm	rm mnt.	rm upp.	rm mid.	rm low
mean [cm]	-6.9	-31.2	-6.8	-1.1	0.3
sdev [cm]	19.5	37.0	12.7	5.0	1.8

Table 3.6: The same as in Tab. 3.5 for 30 h forecast range

	rm	rm mnt.	rm upp.	rm mid.	rm low
mean [cm]	-7.6	-31.1	-7.4	-1.3	0.3
sdev [cm]	20.2	36.9	13.0	5.23	2.0

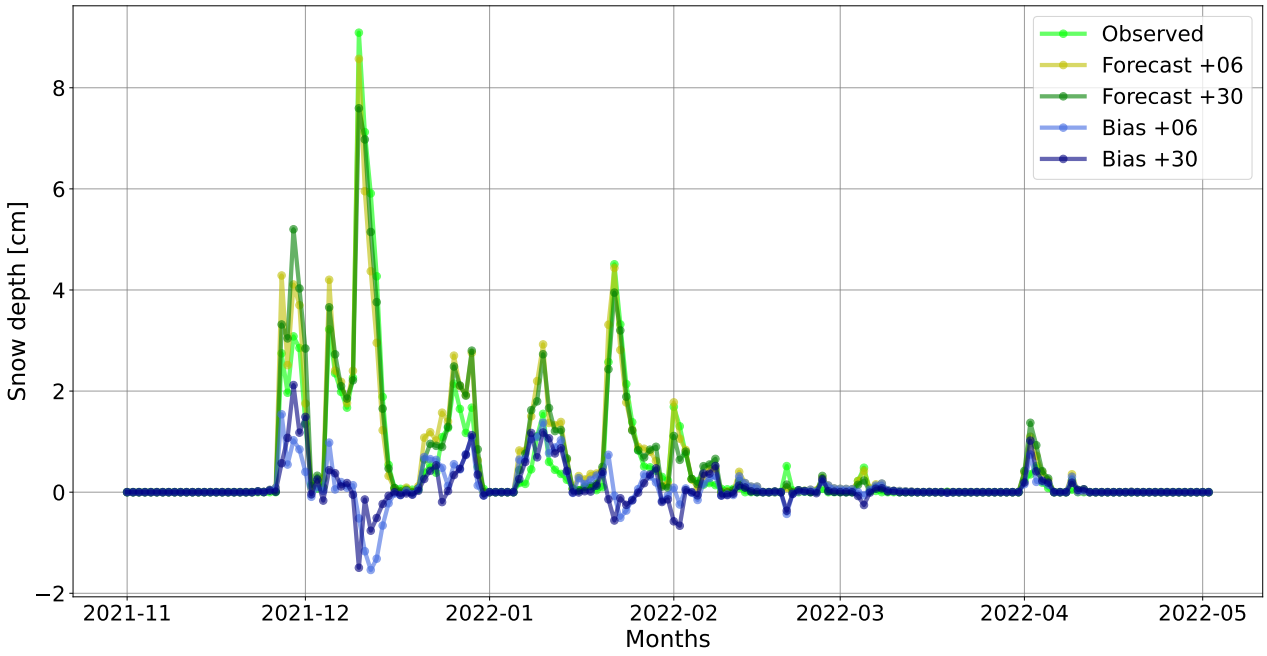

Figure 3.9: Time series of daily snow depth measurements, forecasts and their bias for all regularly measuring stations in low altitudes

The relative value of this positive bias is only 18.9 % and 18.0 % for low altitudes and forecast ranges 6 h and 30 h respectively, which is substantially less than the absolute value of relative bias for regularly measuring mountain stations (80.4 %). Additionally, as can be seen from Fig. 3.11, unlike in the case of mountain stations, daily bias is being dominated by standard deviation for low altitudes. Nevertheless, this tendency to overestimate can be still considered quite important, since, according to the CHMI internal database, altitudes below 400 m cover about 41.7 % of the area of Czechia (Fig. 3.1).

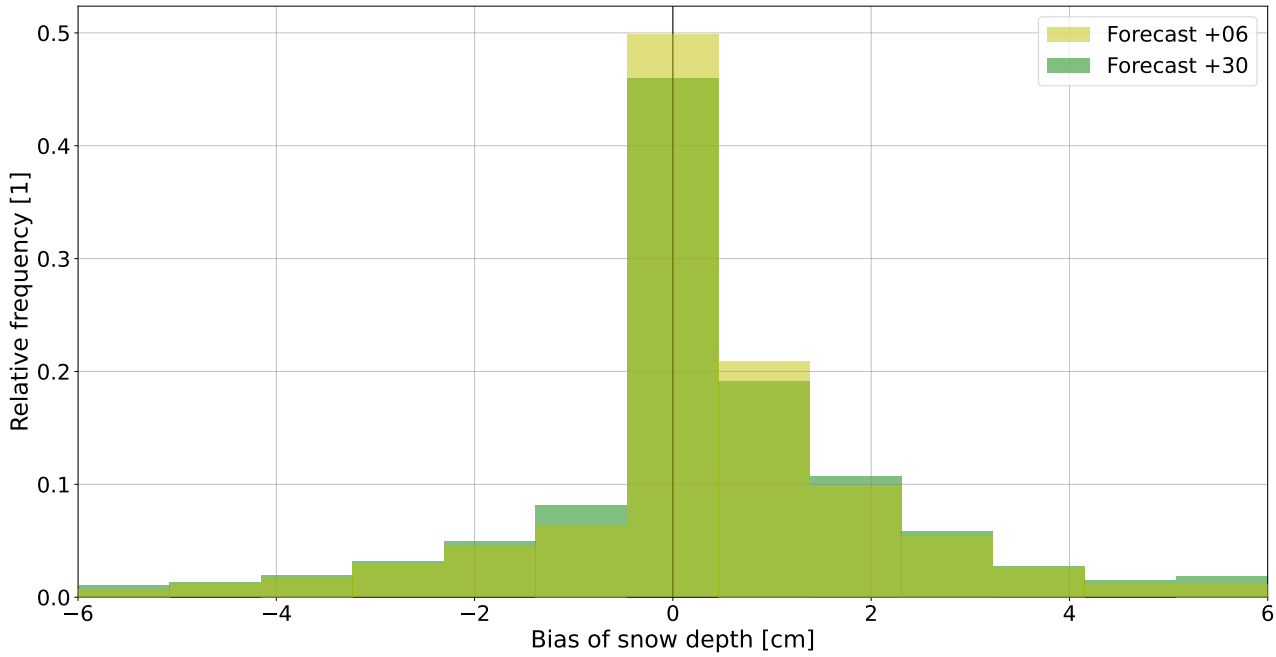

Figure 3.10: Frequency distribution of snow depth forecast bias for stations in low altitudes, at 6 h and 30 h forecast ranges

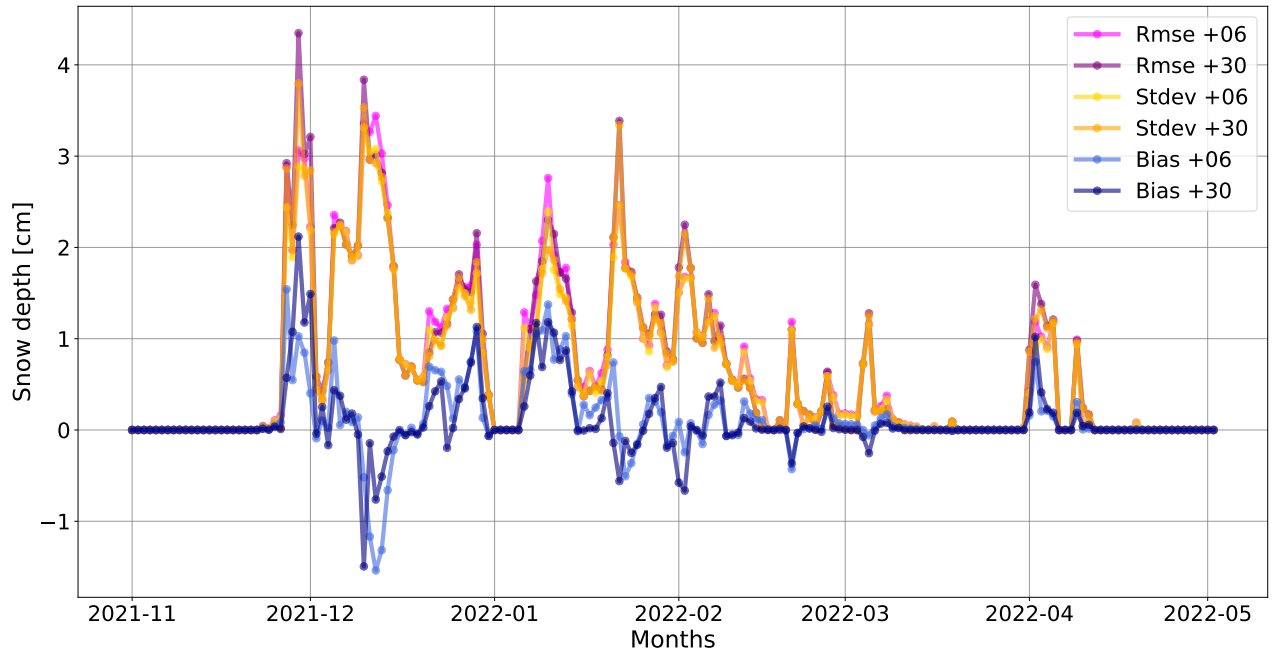

Figure 3.11: Daily time series of used statistical scores for mountain regularly measuring stations

From the perspective of predicting other meteorological elements, for which snow albedo plays a key role, the binary information about counts of forecast false alarms and misses can be interesting. This can neither be seen from any of the shown time series and histograms, nor the scatter plots. Therefore it has been summarized in the form of contingency tables in Fig. 3.12 and Fig. 3.13 for the 6 h forecast range and in Fig. 3.14 and Fig. 3.15 for the 30 h one.

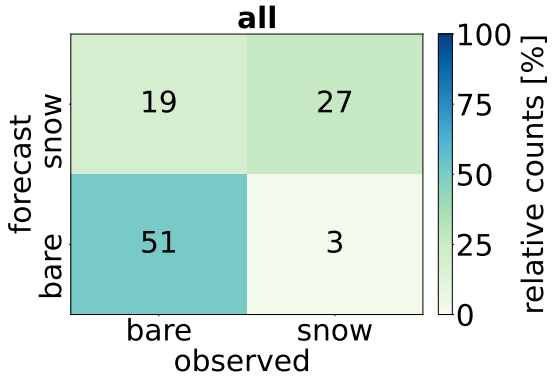

Figure 3.12: Contingency tables showing percentage of accurate forecasts, false alarms and misses of snow depth for regularly measuring stations, at 6 h forecast range

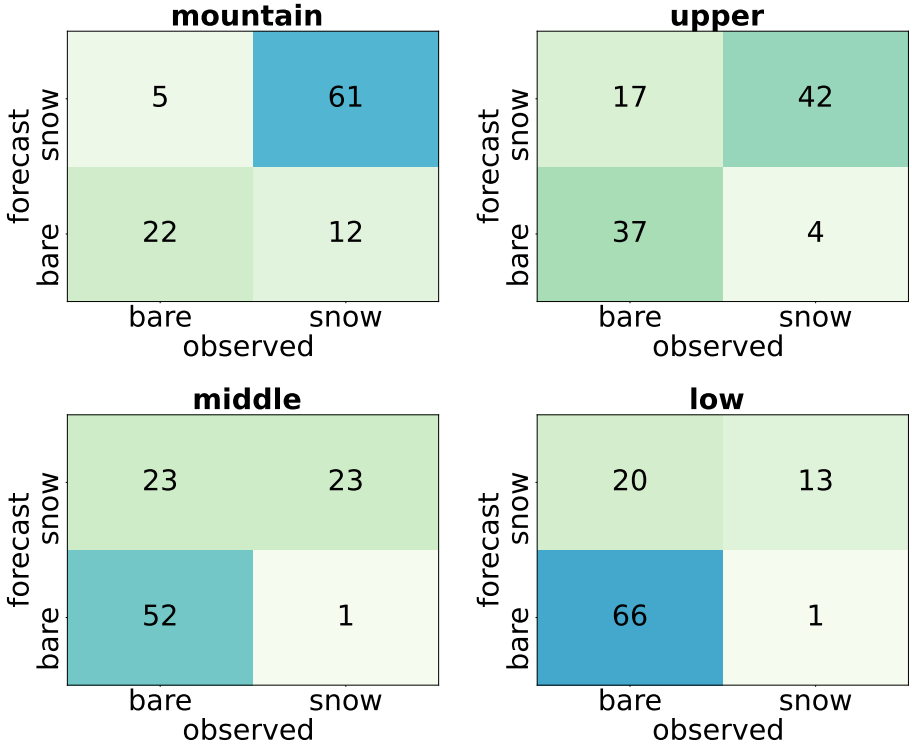

Figure 3.13: Contingency tables showing percentage of accurate forecasts, false alarms and misses of snow depth for stations in different altitude groups, at 6 h forecast range

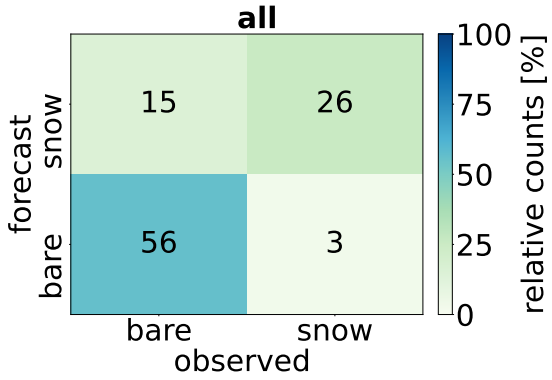

Figure 3.14: Contingency tables showing percentage of accurate forecasts, false alarms and misses of snow depth for regularly measuring stations, at 30 h forecast range

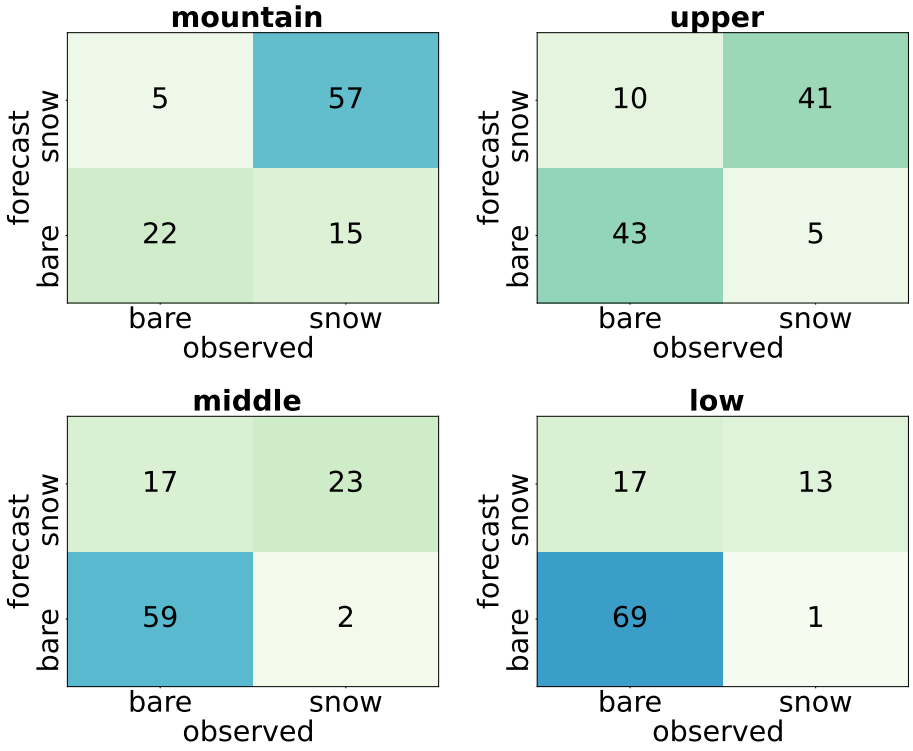

Figure 3.15: Contingency tables showing percentage of accurate forecasts, false alarms and misses of snow depth for stations in different altitude groups, at 30 h forecast range

From the above analysis, it is evident, that bias of snow depth is generally negative. However, from these contingency tables, it can be seen that the number of false alarm cases is greater than the number of misses for all groups except mountain altitudes. In total, false alarms of snow cover make up approximately 15 % of all of the 30 h forecasts and 19 % of the 6 h ones, while missed snow cover only makes up about 3 %. This suggests that any attempt to diminish the underestimation of snow depth should be considered carefully so that the tendency towards false alarms would not get amplified.

Values in the contingency tables are also consistent with the conclusion, that generally, the model is more accurate when forecasting snow depth 30 hours in advance. This is especially true with regard to the number of false alarms, while the tendency for misses is slightly greater for the 30 h forecast range.

As mentioned above, snow depth is not a prognostic variable of ALADIN and the model diagnosed it from snow water equivalent W_s and density ρ_s, according to Eq. (1.9). This makes the causes of the model errors uncertain since one can not clearly say whether the problem lies in snow water equivalent, snow density forecast or possibly both. For that reason, the forecast of snow water equivalent has been validated analogously to snow depth, being the subject of the next section.

3.3 Snow water equivalent validation

3.3.1 Snow water equivalent station analysis

In the case of snow water equivalent verification, weekly data from 410 stations were available. However, only 15 stations have measured regularly every Monday. That means that demanding a constant count of stations, as was the case when dealing with snow depth, would lead to losing about 96.3 % of the original number of stations. This would for example result in the verification of upper stations being made based on data from only 2 stations.

For that reason, the approach based on relative availability of stations has been used again. The value of the availability threshold has been set to 70 %. That means that only stations which provided data on at least 19 Mondays out of the 27 Mondays in the whole winter season have been used. Due to the uneven counts of stations providing data on each Monday, the resulting time series were not homogeneous. However, this approach enabled the usage of 363 stations to find out about the overall trend of the snow water equivalent forecast. Counts of originally available and actually used stations in the same altitude groups, which have been used for snow depth validation, are summarized in Tab. 3.7. The geographic distribution of the stations used for measuring snow water equivalent is in Fig 3.16.

Table 3.7: Counts of stations which measured snow water equivalent at least once, counts of stations measuring on at least 19 Mondays and their percentage of the original number of stations

	total	mountain	upper	middle	low
all stations	410	42	75	161	132
available enough	363	37	66	135	125
percentage [%]	88.5	88.0	88.0	83.9	94.7

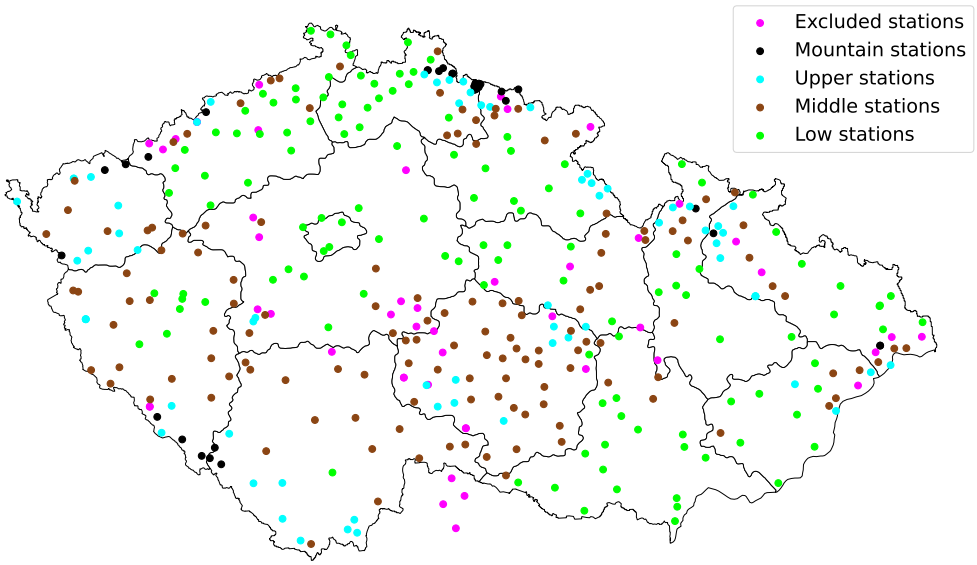

Figure 3.16: Map of excluded and used stations for measuring snow water equivalent, distinguishing 4 altitude categories

3.3.2 Comparison of observed and forecast snow water equivalent

Analogously to the validation of snow depth, measured values of snow water equivalent have been compared to ALADIN 6 h and 30 h forecasts for model grid points closest to each station. The result of this comparison is in Fig. 3.17. It shows the weekly values of observed and forecast snow water equivalent for both forecast ranges, averaged over all stations available on a given Monday. Apart from that, Fig. 3.17 also shows the daily absolute bias of this forecast and counts of available stations in each altitude group. One can see that the average value of snow water equivalent is also significantly underestimated, especially in the last two-thirds of the winter season.

From comparison with Monday time series of snow depth in Fig 3.18, it can be seen that the behaviour of average W_s and average d_s is fairly similar. That holds except for the two peaks, which appear at the beginning of March and April in the time series of the former. These peaks do not correspond to the actual physical situation but are caused by a change in the count of measuring stations. They appear on days with a smaller number of stations. As is evident from the barplots in Fig. 3.17, the decline is the most significant in the case of the number of middle and upper stations, while the number of mountain stations remains almost constant. Then, suppose that the mountain stations contribute to the average more than the middle and upper ones, the sum of snow water equivalent on these days would not decrease as much as the station count. This station count is being used for normalization of the sum of W_s, which causes the average to rise. The assumption that mountain stations contribute to the average more strongly than the middle and upper ones is reasonable, considering Fig. 3.3, which shows that in the last third of winter, the average snow depth was significantly higher for mountain altitudes than for all the other groups.

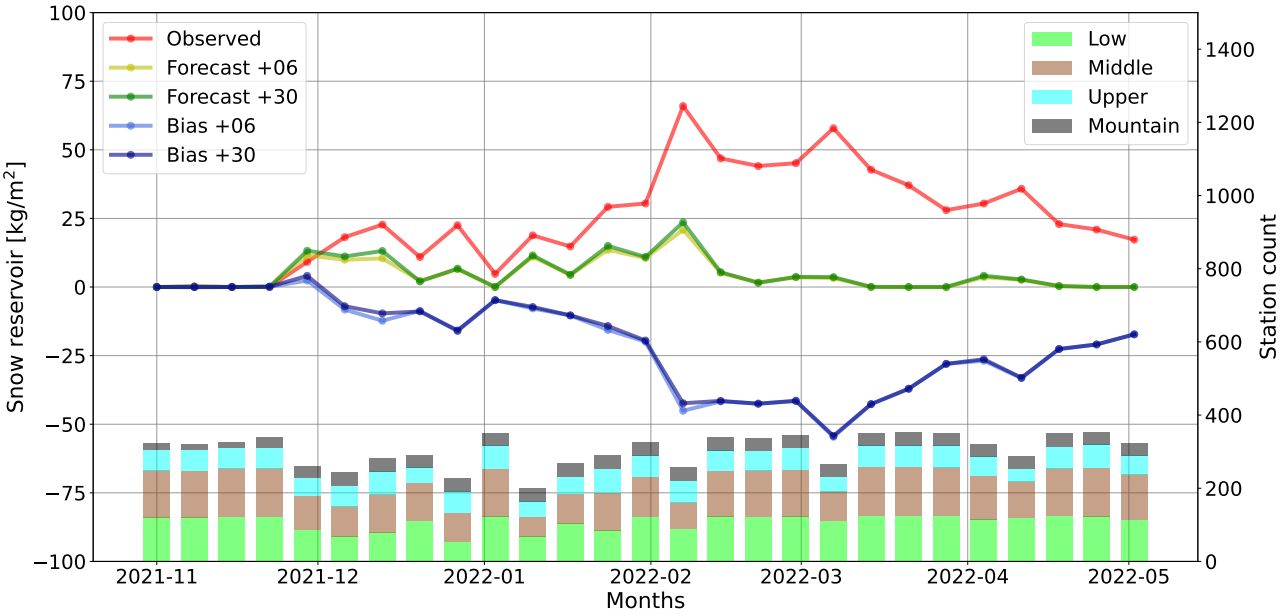

Figure 3.17: Weekly time series of snow water equivalent measurements and forecasts, averaged over all available-enough-stations, absolute bias and daily counts of available stations, at forecast ranges 6 and 30 hours

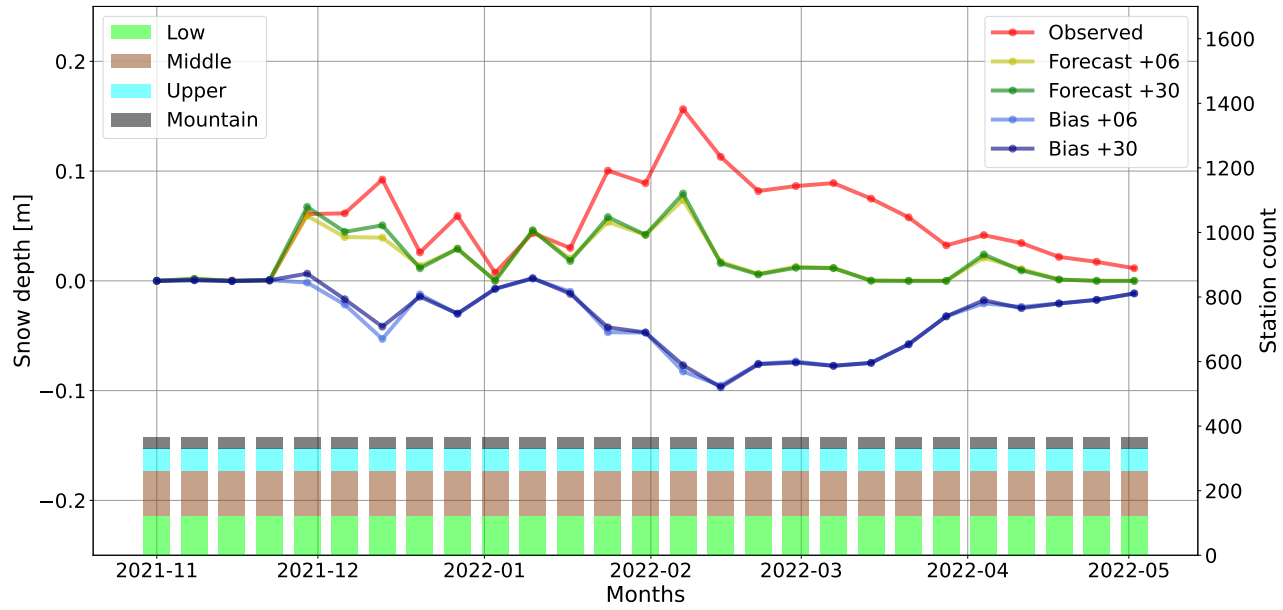

Figure 3.18: Time series of average weekly observed and forecast values of snow depth, forecast bias and counts of regularly measuring stations, at forecast ranges 6 and 30 hours

From Fig. 3.17 it can be seen, that the non-constant number of stations caused the peaks to appear in the case of observations but not in the case of the forecast.

This suggests that the forecast values of snow water equivalent were closer to each other for the different altitude groups, which made the decrease in station count less problematic in terms of affecting the average. From this it follows, that there have to be differences in relative bias of W_s forecast among the altitude groups.

Analogously to snow depth, the dependency of forecast performance on altitude was examined for snow water equivalent as well. A general idea about the accuracy of snow water equivalent forecast for different altitudes can be made from scatter plots in Fig. 3.19. They show that the model bias is greater when underestimating snow water equivalent in mountain, upper and middle altitudes, while such tendency is not observed in the case of stations situated lower.

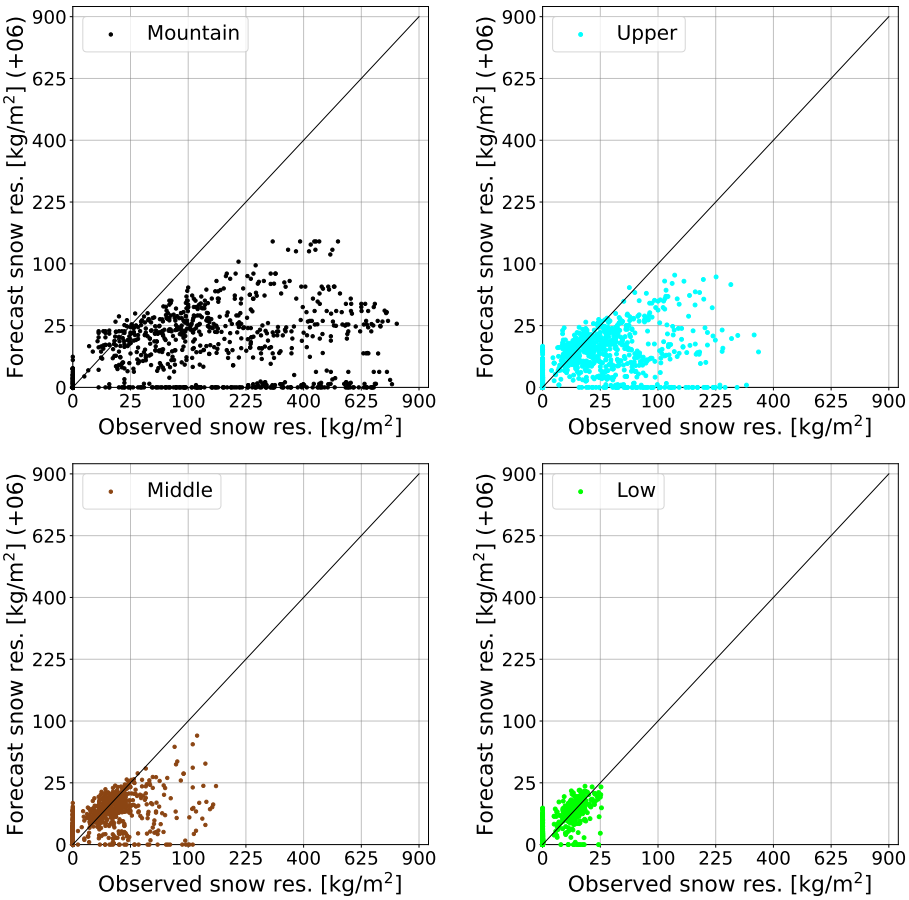

Figure 3.19: Scatter plots comparing forecast and observed snow water equivalent for different altitude groups, both axes with square root scale, at 6-hour forecast range

Some more precise conclusions can be made from the results of all the mentioned statistical scores (see Tab. 3.8, Tab. 3.9). The values of absolute bias show that the model underestimates snow water equivalent on average, as well as in the case of mountain, upper and middle altitudes. In the case of low stations, the model tends to overestimate it.

From the values of relative bias, it is clear that the systematic error of the forecast gets less significant with decreasing altitude, which is the same behaviour that has been seen when validating snow depth forecast. However, the systematic error of W_s forecast averaged over all available stations is roughly 20 % larger than the one of d_s in the case of both forecast ranges. Additionally, W_s forecast seems

to be more biased than snow depth forecast even in the case of all the separated groups except the low altitudes.

This could be partly due to the values of bias being enlarged by the mentioned peaks originating from the non-constant station count (Fig. 3.20). However, the underestimation of W_s is more significant than the one of d_s even in the case of mountain stations and for these remains the number of stations almost constant (see Fig. 3.21). This leads to the conclusion, that in the case of mountain and possibly upper and middle stations, the underestimation of snow depth has not only been caused by the underestimation of snow water equivalent, but it must have been partially compensated by the forecast values of density being too low. That is the subject of Section 3.4.

Table 3.8: Values of used statistical characteristics for all available enough (denoted avl) stations together and split accordingly to altitudes, at 6 h forecast range

	avl	avl mnt.	avl upp.	avl mid.	avl low
B [kg m^{-2}]	-21.00	-159.62	-17.57	-1.97	0.07
$B^{(r)}$ [%]	-84.0	-90,0	-74.4	-49.4	7.8
Σ [kg m^{-2}]	81.79	191.94	42.12	11.89	1.73
Δ [kg m^{-2}]	84.44	249.64	45.64	12.05	1.73

Table 3.9: The same as in Tab. 3.8 for 30 h forecast range

	avl	avl mnt	avl upp.	avl mid.	avl low
B [kg m^{-2}]	-20.60	-157.93	-17.04	-1.76	0.19
$B^{(r)}$ [%]	-82.4	-89.1	-72.1	-44.1	24.8
Σ [kg m^{-2}]	81.38	191.50	41.86	11.78	1.92
Δ [kg m^{-2}]	83.95	248.23	45.20	11.91	1.93

The conclusion that ALADIN underestimates snow water equivalent in mountain, upper and middle altitudes is also supported by results of the analysis of bias frequency distribution. The mean values of these distributions are negative in the case of all station groups except the low altitudes. They are summarized in Tab. 3.10 and Tab. 3.11, together with standard deviation of these distributions. The zero values of bias corresponding to correct forecasts of no snow water equivalent have been left out, the same as in the case of snow depth.

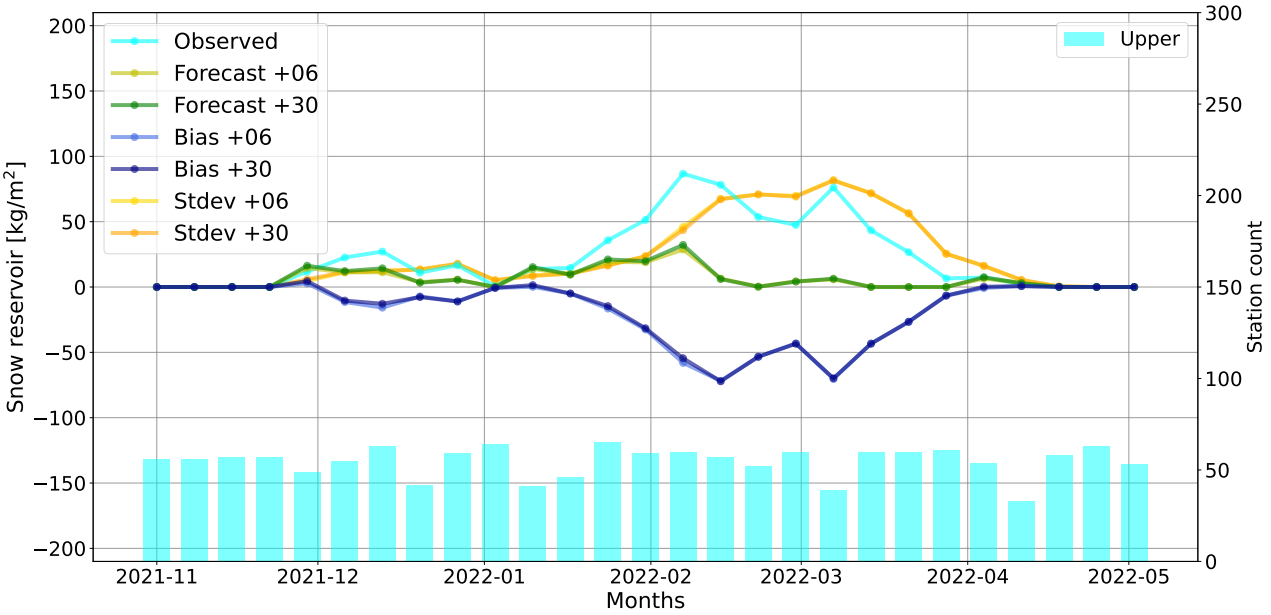

Figure 3.20: Time series of observed and forecast snow water equivalent averaged over all stations in upper altitudes, forecast bias and standard deviation, at 6 and 30-hour forecast ranges, barplots with counts of available stations

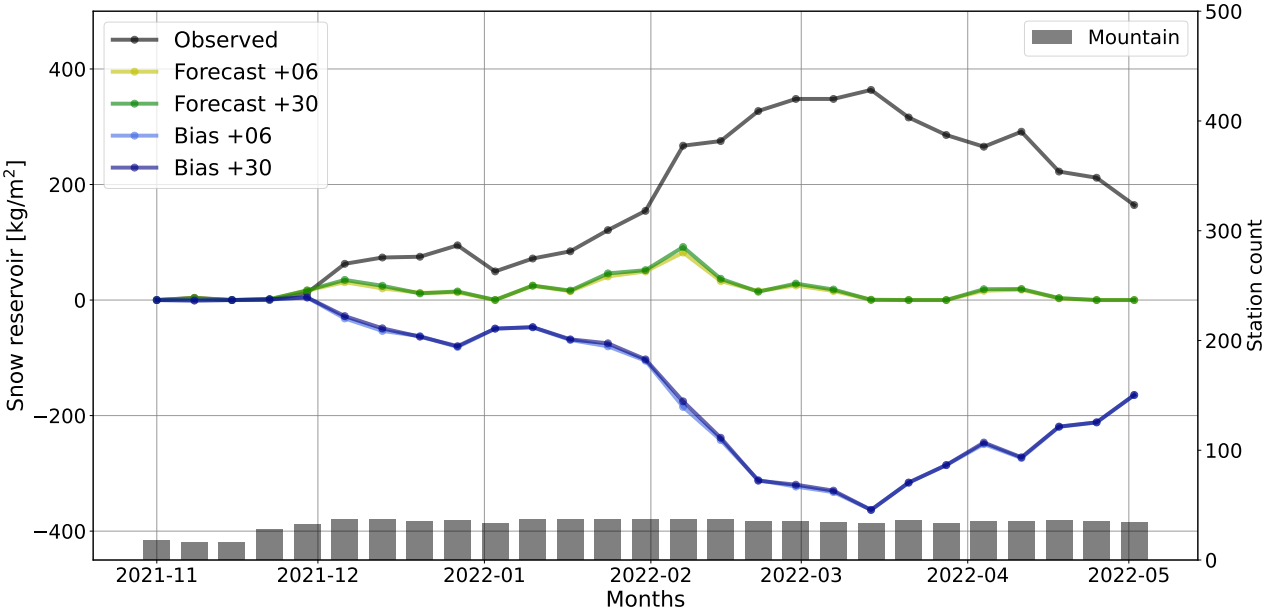

Figure 3.21: Time series of observed and forecast snow water equivalent averaged over all stations in mountain altitudes, forecast bias, 6 and 30-hour forecast ranges, barplots with counts of available stations

The mean values of bias distributions cannot be used for comparing d_s and W_s forecast. That is because the value of ρ_s for these mean values is unknown. However, the shape of the bias distributions can be compared, if they originate from equivalent data sets. By equivalent data sets are meant observations and

Table 3.10: Mean and standard deviation of snow water equivalent forecast bias distributions for all altitude groups, at 6-hour forecast range, (avl denotes available enough stations)

	avl	avl mnt.	avl upp.	avl mid.	avl low
mean [$\mathrm{kg\,m^{-2}}$]	-47.58	-182.10	-28.43	-4.94	0.26
sdev [$\mathrm{kg\,m^{-2}}$]	117.87	194.77	50.62	18.45	3.36

Table 3.11: The same as in Tab. 3.10 for 30 h forecast range

	avl	avl mnt.	avl upp.	avl mid.	avl low
mean [$\mathrm{kg\,m^{-2}}$]	-52.74	-180.64	-30.77	-5.43	0.82
sdev [$\mathrm{kg\,m^{-2}}$]	123.52	194.54	52.37	20.23	3.94

forecasts of such stations, which measured both snow depth and snow water equivalent simultaneously. Additionally, the cases of correct forecast of no snow cover have been excluded from these data sets. These distributions are plotted in Fig. 3.22 and Fig. 3.23. Their comparison shows that the distribution of snow depth bias is indeed less shifted towards negative values than the one of snow water equivalent bias. However, corresponding ranges for W_s and d_s in the plots are only obtained by assuming snow density of $200\,\mathrm{kg\,m^{-3}}$.

Forecast of W_s for low stations is overestimated. That can be seen from its positive bias for low stations (see Tab. 3.8, Tab. 3.9). The mean of bias for low stations (Tab. 3.10, Tab. 3.11) is also positive and the time series in Fig. 3.24 shows the same trend. Unlike in the case of all the other groups and in the case of snow depth, the accuracy of W_s forecast in low altitudes differs with the forecast range quite significantly. Its relative bias is 17 % smaller for the 6 h forecast range than relative bias for the 30 h one. However, as is apparent from Fig. 3.24, this difference in the performance of the model between the two forecast ranges is not very statistically significant. That is due to the weakly frequency of snow water equivalent measurements and also due to the lack of snow in low altitudes during the second half of the winter season.

From the seasonal values of standard deviation and root mean square error of snow water equivalent forecast, it is evident, that the random component of model error tends to outbalance the systematical one as altitude decreases, the same as it is in the case of snow depth (see Tab. 3.8, Tab. 3.9). This is well illustrated in Fig. 3.25, where the time series of low stations standard deviation dominates daily bias and makes up the main component of daily root mean square error. In the case of upper stations, the daily magnitudes of bias and standard deviation are comparable, see Fig. 3.20. For mountain stations forecast, the daily values of bias are greater than the values of standard deviation, as is obvious from Fig. 3.26. From this, it follows, that in the case of mountain stations, the value of standard deviation averaged over the whole winter season Σ is greater than the value of bias B only thanks to the interdiurnal variability being taken into account by Σ. That was also the case with snow depth forecast.

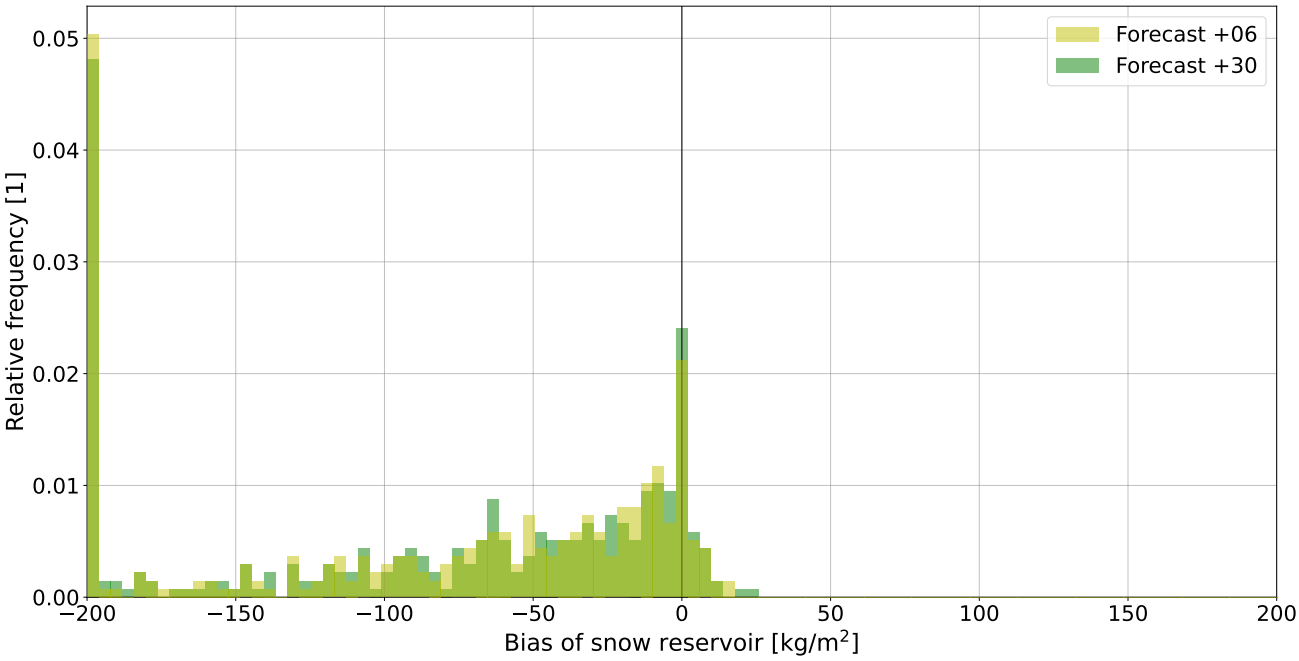

Figure 3.22: Frequency distribution of snow water equivalent forecast bias for stations in mountain altitudes, measurements comparable with snow depth, 6 h and 30 h forecast ranges

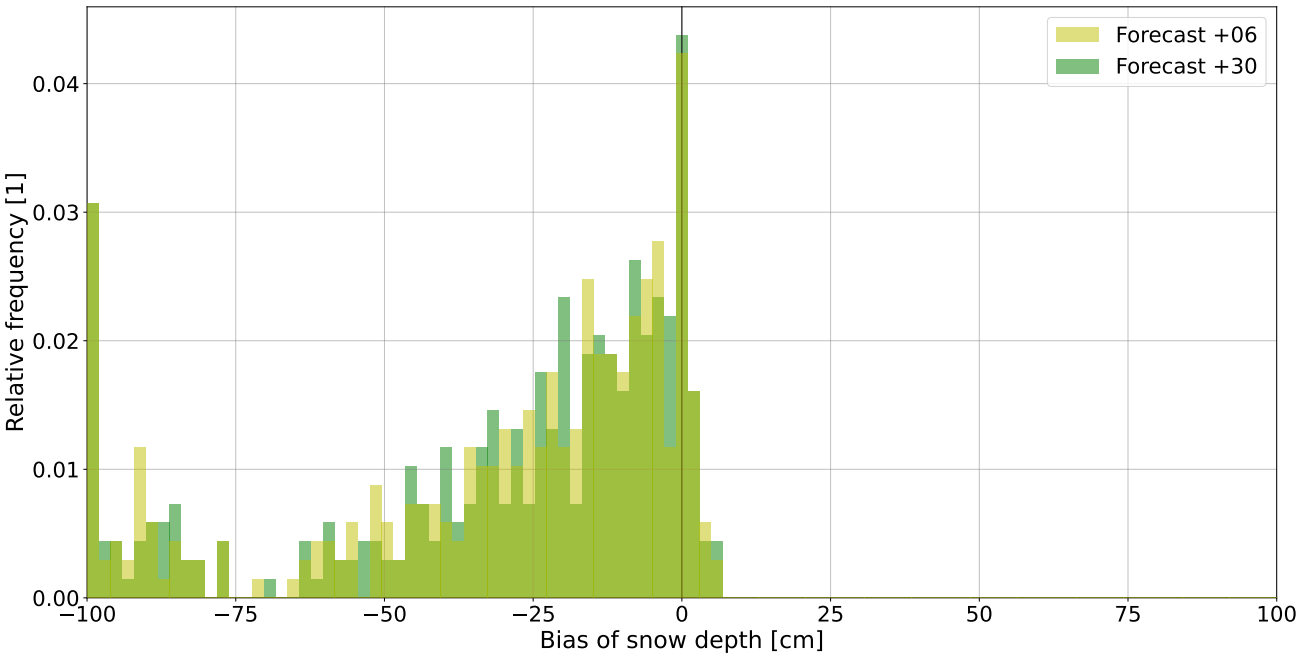

Figure 3.23: The same as in Fig. 3.22 for snow depth forecast

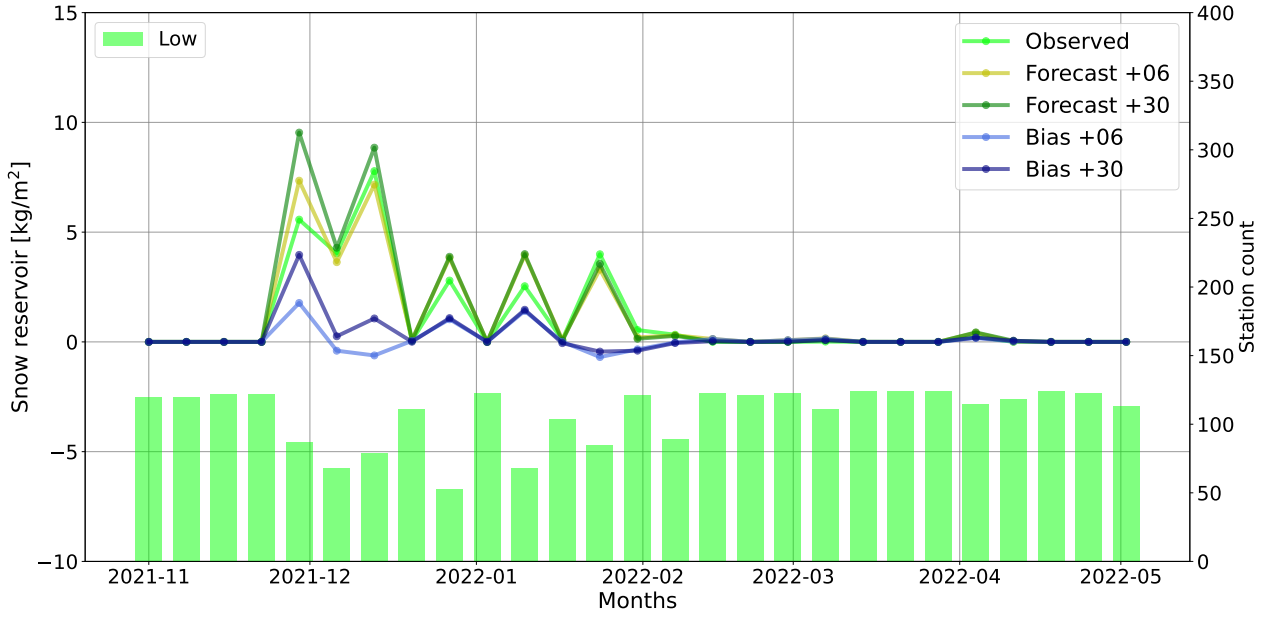

Figure 3.24: Time series of observed and forecast snow water equivalent averaged over all stations in low altitudes, forecast bias, 6 and 30-hour forecast ranges, barplots with counts of available stations

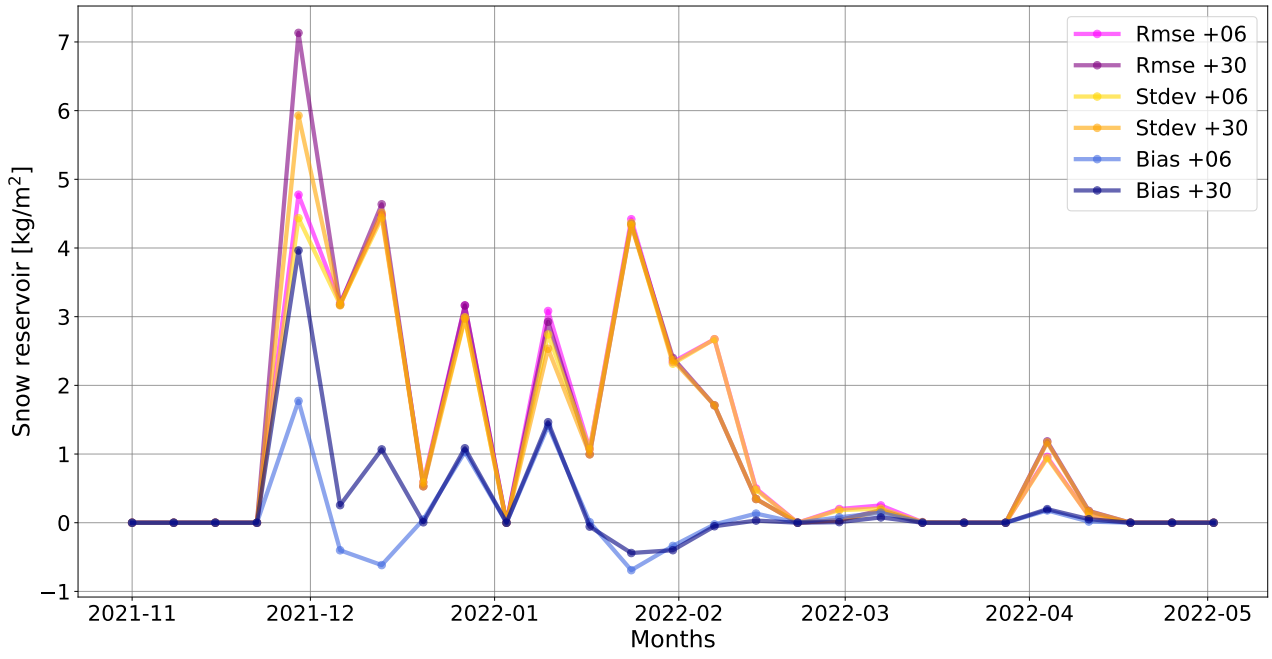

Figure 3.25: Weekly time series of used statistical scores for available enough, W_s-measuring stations in low altitudes, at 6 and 30 h forecast ranges

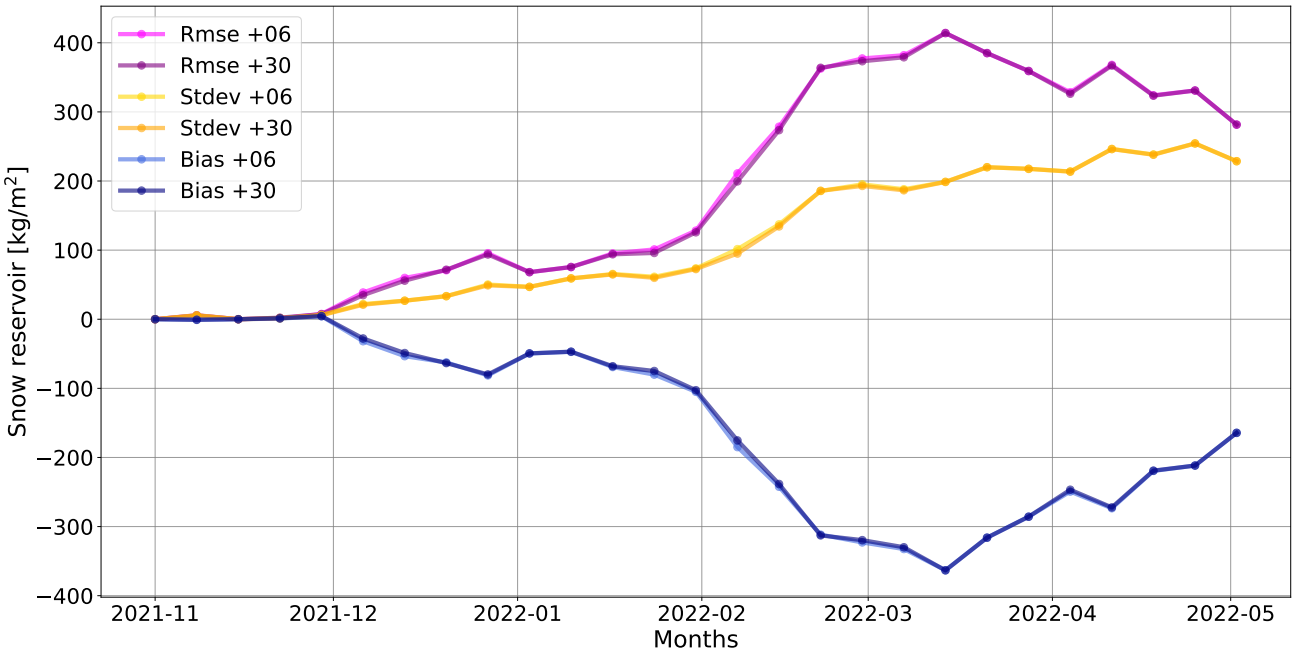

Figure 3.26: Weekly time series of used statistical scores for available enough, W_s-measuring stations in mountain altitudes, at 6 and 30 h forecast ranges

The analysis of snow water equivalent concerning false alarms and misses is summarized in Tab. 3.27 and Tab. 3.28 for the 6 h forecast range. For the 30 h one it is in Tab. 3.29 and Tab. 3.30. Not very surprisingly, it shows the same general trends which hold for snow depth. These are an overall tendency towards false alarms over misses of non-zero snow water equivalent forecast. This tendency is also present for all altitude groups except mountain stations. For those, the number of misses is greater.

Theoretically, the percentages in these contingency tables should be the same for snow water equivalent and snow depth, since naturally, neither of these quantities can occur without the other one. Even in the case of forecast values, snow depth is calculated directly from snow water equivalent. Yet there are some obvious differences between the percentages of false alarms and misses of snow depth and snow water equivalent forecast for all used stations (compare Tab. 3.12 and Tab. 3.27) and also for the station groups evaluated separately (compare Tab. 3.13 and Tab. 3.28). These are most probably caused by differences between the original data sets due to the station sets not being the same for d_s and W_s. Another possible reason for such differences could be, that regular climatological stations measure snow water equivalent in case of snow depth greater than 4 cm. This would lead to an increase in alleged false alarms of snow water equivalent forecast relative to snow depth forecast. However, this is exactly the opposite trend than the one shown by the contingency tables. This means that this phenomenon has either been compensated by the mentioned differences between the data sets, or the methodology of snow water equivalent measurements is not being followed strictly.

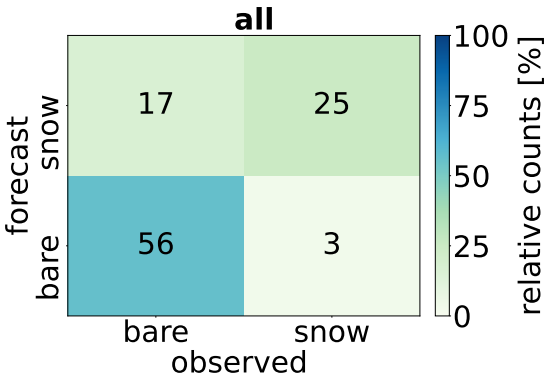

Figure 3.27: Contingency tables showing percentage of accurate forecasts, false alarms and misses of snow water equivalent forecast for regularly measuring stations, at 6 h forecast range

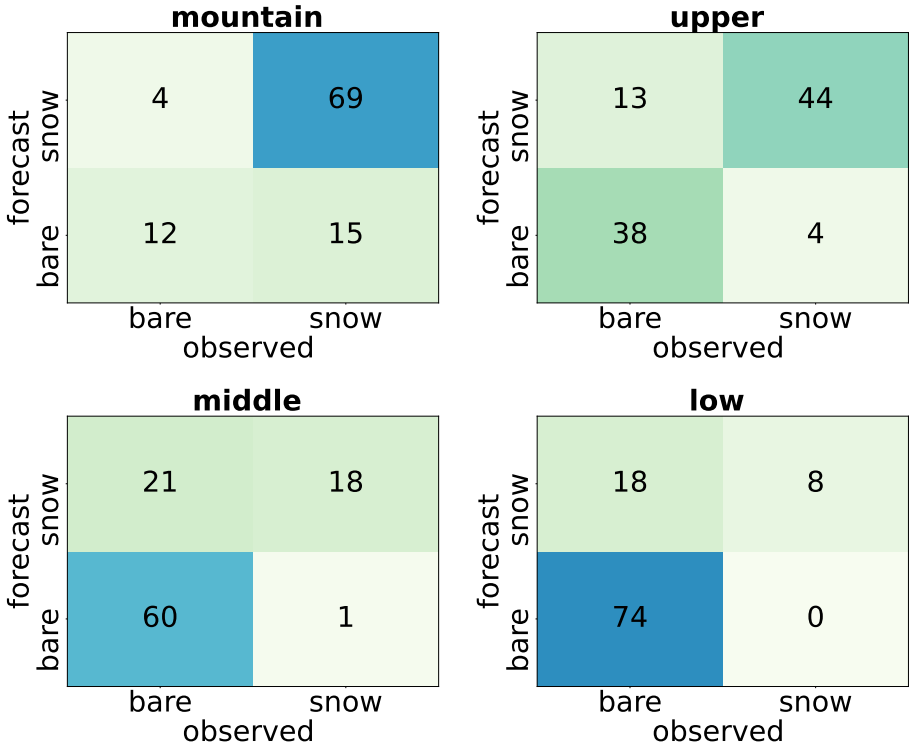

Figure 3.28: Contingency tables showing percentage of accurate forecasts, false alarms and misses of snow water equivalent forecast for stations in different altitude groups, at 6 h forecast range

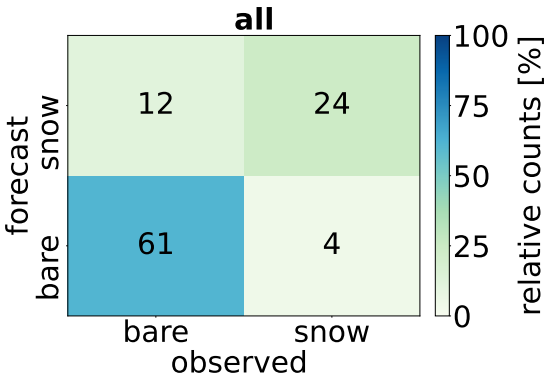

Figure 3.29: Contingency tables showing percentage of accurate forecasts, false alarms and misses of snow water equivalent forecast for regularly measuring stations, at 30 h forecast range

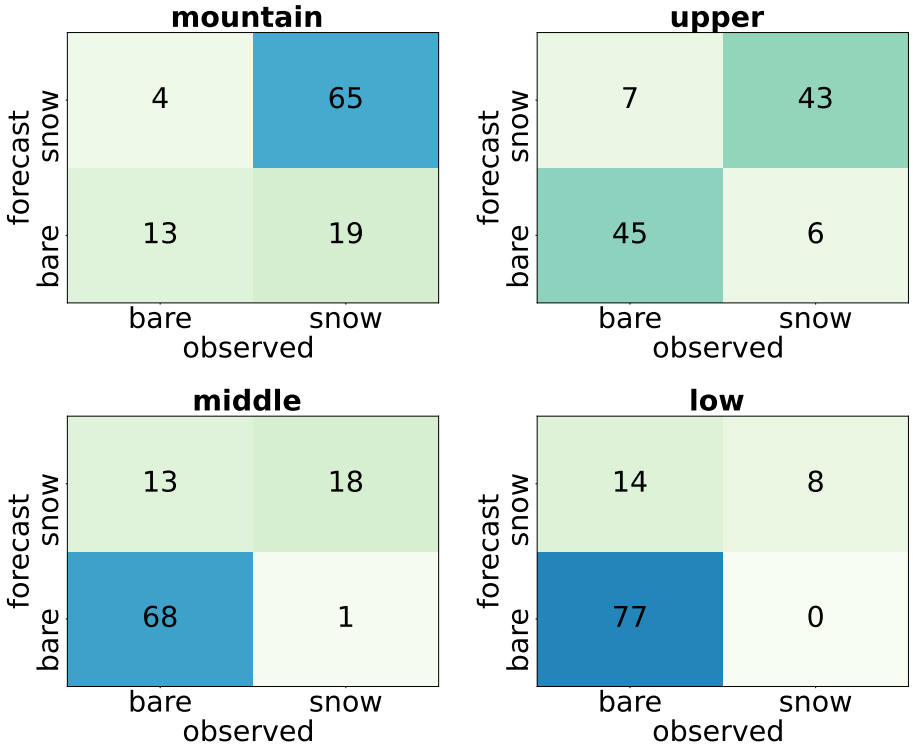

Figure 3.30: Contingency tables showing percentage of accurate forecasts, false alarms and misses of snow water equivalent for stations in different altitude groups, at 30 h forecast range

3.4 Snow density validation

Snow density is not being directly measured on regular meteorological stations as often as snow depth and water equivalent are. For that reason, it had to be calculated from measured snow depth and snow water equivalent using Eq. (1.9). Because of this, only data from stations which measured both W_s and d_s on one day could be used. For consistency with the rest of the validation, these stations were only picked from the intersection of the set of stations regularly measuring d_s and the set of stations available enough for W_s measurements.

Additionally, measurements of non-physical values of density were taken out of the data set. By non-physical are meant those values of density, which lie outside the interval $[50, 830]\,\mathrm{kg\,m^{-3}}$. This interval represents the possible values of snow density according to Cuffey and Paterson [2010]. These non-physical values occurred in the data set due to incorrect values of snow depth or snow water equivalent, which were not outliers on their own, but their combination in Eq. (1.9) produced unreasonable results. Another condition requires a non-zero value of snow water equivalent in the model. All these conditions have lowered the number of useful stations, especially at the end of the winter season, when there was little forecast snow.

The result of this analysis is in Fig. 3.31, showing that the density forecast is quite accurate in the first half of the winter season. However, it tends to be underestimated in the second half, when snow is mostly present in mountain and upper altitudes and had settled over time. This is consistent with the conclusions from Subsection 3.3.2, that when forecasting d_s, the underestimation of W_s is partly compensated by the underestimation of snow density ρ_s in the case of mountain altitudes.

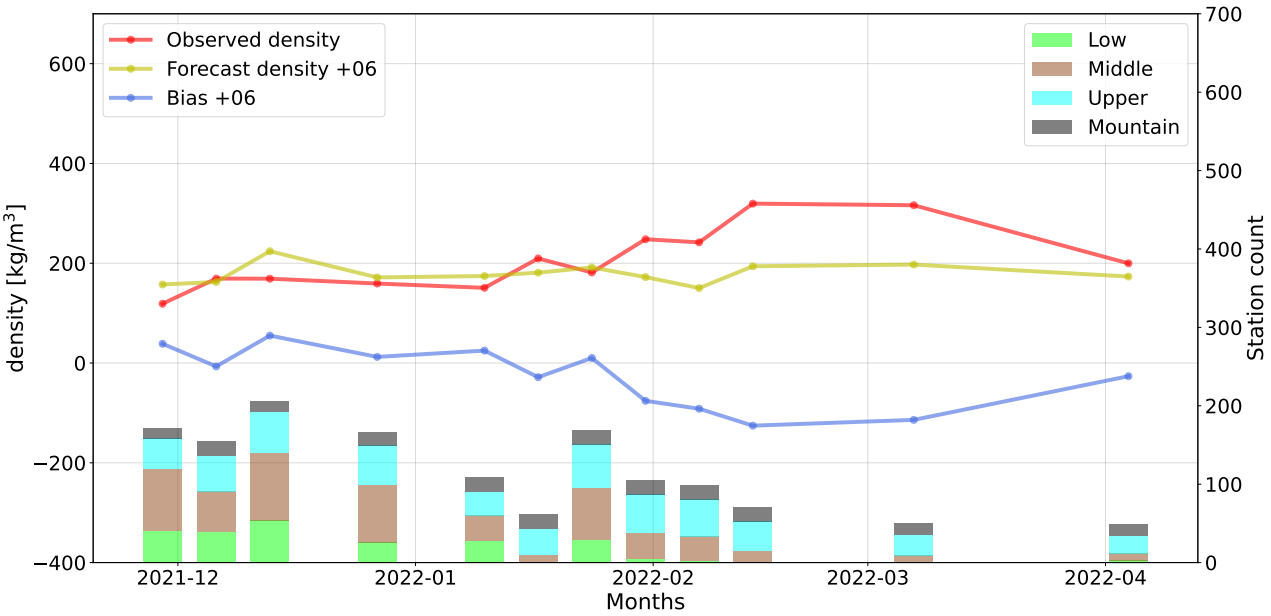

Figure 3.31: Time series of observed and forecast density, absolute bias, barplots with counts of available stations, at 6 h forecast range

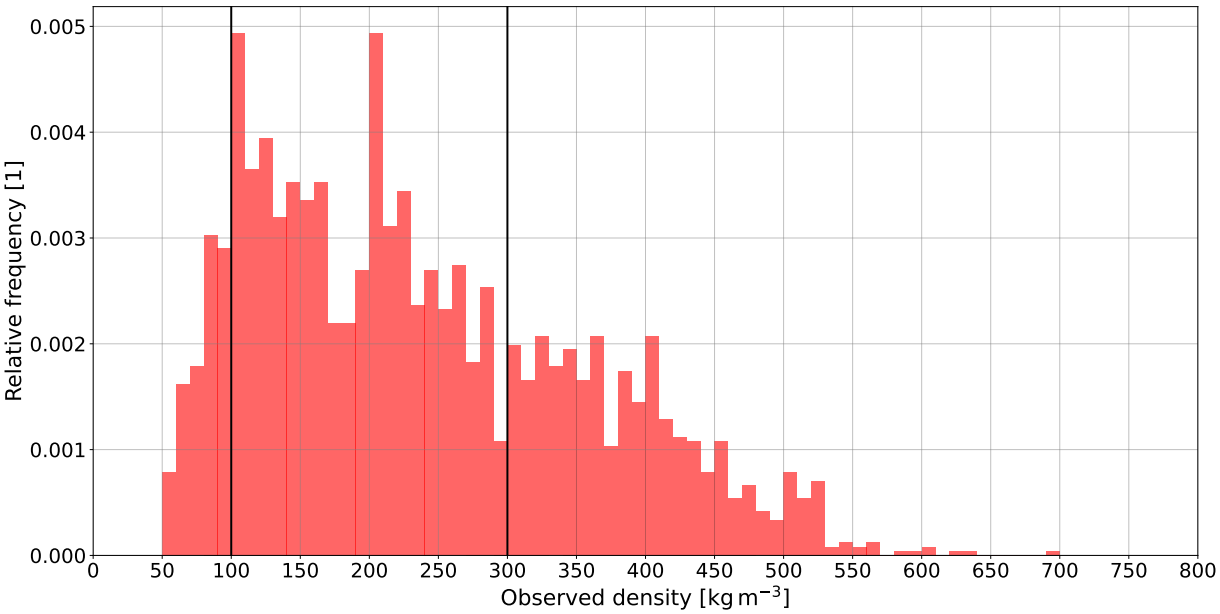

Figure 3.32: Histogram showing the distribution of observed density of snow

The result is also consistent with the limits of model snow density introduced in subsection 1.1.3 being $\rho_s^{min} = 100\,\mathrm{kg\,m^{-3}}$ and $\rho_s^{max} = 300\,\mathrm{kg\,m^{-3}}$. If one considers the above-mentioned values, which snow density can actually have according to Cuffey and Paterson [2010], it is evident that the model cannot forecast the values of snow density characteristic for settled snow and firn at the end of the winter season. This is illustrated by the histogram in Fig. 3.32, which shows that the measured values of density indeed do not fit into the model limits. The histogram only serves as an illustration of the range of values density can have. Therefore, its data set has not been constrained by any of the previous conditions, except for the exclusion of non-physical values.

Conclusion

The aim of this thesis was first to get acquainted with snow parametrization of model ALADIN in the configuration used at CHMI. It is described by equations, which have been taken from several resources, compared to the model code and summarized in Chapter 1. Primarily, they describe the way of computing the time tendency of snow-related prognostic variables: snow reservoir represented by snow water equivalent W_s, snow albedo A_s and snow density ρ_s. They also deal with diagnosing additional snow characteristics: snow depth d_s and snow fraction f_s. Direct correspondence of these symbolic equations with the model code is in the attachments chapter in Section A.1.

Chapter 2 presents the station network in Czechia and summarizes the methodology of measuring snow-related variables W_s and d_s.

The main focus of the thesis was the validation of model snow-related variables. For that, observations of snow depth and snow water equivalent from winter season 2021/2022 have been compared to corresponding forecasts. Forecast ranges 6 and 30 hours have been selected. This has been done in sections 3.2 - 3.4.

Along the validation, some specifics about the snow-measuring station network have been found. These relate for example to the availability of the stations and their influence on the average time series. Another outcome of the validation are several verification tools based on Python scripts, which could potentially be helpful for further work.

The results of this validation are following: The model underestimates forecast of both snow depth and snow water equivalent in altitudes above 400 m a.s.l. The magnitude of this underestimation gets greater with rising altitude. In altitudes below 400 m a.s.l., d_s and W_s are both overestimated, but this bias is the lowest from all the altitude groups. There is no significant difference in accuracy between the 6 h and 30 h forecast ranges. From comparison of W_s and d_s forecasts, prediction of snow water equivalent comes out as the more negatively biased one in altitudes above 400 m a.s.l. In agreement with that, snow density was found to be underestimated in the case of higher altitudes and older snowpack. Averaged over all altitudes, the forecast of density turned out to be quite accurate. However, the interval limiting forecast density is too narrow, compared to observations and theory.

From the perspective of predicting snow occurrence, the overall tendency of the model is towards false alarms. That holds for all altitudes except stations above 800 m a.s.l. In their case the number of misses is greater. These results are valid for both snow depth and snow water equivalent.

Possible cause of the model error could be in the determination of the initial condition. According to Bučánek et al. [2015], the initial condition for snow-related variables is taken from the previous 6 h forecast. For security, a weak relaxation of 4.5 % towards climatological characteristics is made. No assimilation of observed data is being made, unlike in the case of other meteorological variables. That leaves space for potential future improvement.

Bibliography

E. Bazile, M. ElHaiti, A. Bogatchev, and V. Spiridonov. Improvement of the snow parametrization in ARPEGE/ALADIN, 2001.

J. Bednář and O. Zikmunda. *Fyzika mezní vrstvy atmosféry*. Academia, Prague, 1985.

R. Brožková, A. Bučánek, J. Mašek, P. Smolíková, and A. Trojáková. Nová provozní konfigurace modelu aladin ve vysokém rozlišení. *Meteorol. zprávy*, 72(5):129–139, 2019.

A. Bučánek, A. Trojáková, and R. Brožková. Asimilačí schéma BlendVar v ČHMÚ. *Meteorol. zprávy*, 68(6):180–185, 2015.

J. Coiffier. *Fundamentals of Numerical Weather Prediction*. Cambridge University Press, The Edinburgh Building, Cambridge CB2 8RU, UK, 2011. ISBN 978-1-107-00103-9.

K.M. Cuffey and W.S.B. Paterson. *The Physics of Glaciers*. Elsevier, Inc., 30 Corporate Drive, Suite 400, Burlington, MA 01803, USA, 2010. ISBN 978-0-12-369461-4.

H. Douville, F. Royer, and F. Mahouf. A new snow parametrization for the Méteó-France climate model part I: validation in stand alone experiments. *Climate Dynamics*, 12(1):21–35, 1995.

L. Gerard. Physical Parameterizations in Arpege-Aladin operational model. `https://www.umr-cnrm.fr/gmapdoc/spip.php?article12`, June 2005.

F.E. Hewer and N. Wood. The effective roughness length for scalar transfer in neutral conditions over hilly terrain. *Quarterly journal of the royal meteorological society*, 124:659–685, 1998.

P. Lipina, M. Řepka, and V. Šustková. Meteorologická staniční síť ČHMÚ v roce 2020. *Meteorologické zprávy*, 35(1):149–164, 2021.

P. Lipina, I. Kain, J. Jirák, Š. Bercha, and D. Židek. *Návod pro pozorovatele automatizovaných meteorologických stanic*. 13a. ČHMÚ, Praha, 2022.

J. Mašek. Improved treatment of surface roughness in the ISBA scheme. pages 1–13, 2018.

A. Ridgen, D. Li, and Salvucci G. Dependence of thermal roughness length on friction velocity across land cover types: A synthesis analysis using ameriflux data. *Agricultural and Forest Meteorology*, 249:512–519, 2017.

P. Termonia, C. Fischer, E. Bazil, F. Bouyssel, R. Brožková, P. Bénard, B. Bochenek, D. Degrauwe, M. Derková, R. El Khatib, R. Hamdil, J. Mašek, P. Pottier, N. Pristov, Y. Seity, P. Smolíková, O. Španiel, M. Tudor, Wittman Ch. Wang, Y., and A. Joly. The ALADIN System and its canonical model configurations AROME CY41T1 and ALARO CY40T1. *Geoscientific Model Development*, 11:257–281, 2018.

Česká meteorologická společnost. Elektronický meteorologický slovník. http://slovnik.cmes.cz/. Accessed: 2023-04-14.

List of Figures

1.1 Schematic view describing various reservoirs and fluxes in the ISBA scheme, an image courtesy of Luc Gerard (Gerard [2005]). Notation in the scheme is derived from French. However, further in the text, these English-derived equivalents will be used: snow reservoir $S_n \rightarrow W_s$, snow melting flux $F_n \rightarrow F_m$, flux from solid reservoirs $F_{evn} \rightarrow F_{evs}$ 4

1.2 A diagram illustrating the relationship between snow depth and snow reservoir 6

3.1 Map of excluded and used snow-depth-measuring stations distinguishing 4 altitude categories 12

3.2 Daily time series of observed and forecast snow depth, averaged over all regularly measuring stations and their absolute bias, at forecast ranges 6 and 30 hours 13

3.3 Daily time series of observed snow depth averaged over different altitude groups 13

3.4 Scatter plots comparing forecast and observed snow depth for different altitude groups, both axes with square root scale, at 6 h forecast range 15

3.5 Time series of daily snow depth measurements, forecasts and their absolute bias for all regularly measuring stations in mountain altitudes 16

3.6 Time series of weekly snow depth measurements, forecasts and their absolute bias for all stations in mountain altitudes, barplots with counts of stations available on the day of measurement . . . 17

3.7 Daily time series of used statistical scores for mountain regularly measuring stations 17

3.8 Frequency distribution of snow depth forecast bias for regularly measuring stations in mountain altitudes, at 6 h and 30 h forecast ranges 18

3.9 Time series of daily snow depth measurements, forecasts and their bias for all regularly measuring stations in low altitudes 19

3.10 Frequency distribution of snow depth forecast bias for stations in low altitudes, at 6 h and 30 h forecast ranges 20

3.11 Daily time series of used statistical scores for mountain regularly measuring stations 20

3.12 Contingency tables showing percentage of accurate forecasts, false alarms and misses of snow depth for regularly measuring stations, at 6 h forecast range 21

3.13 Contingency tables showing percentage of accurate forecasts, false alarms and misses of snow depth for stations in different altitude groups, at 6 h forecast range 21

3.14 Contingency tables showing percentage of accurate forecasts, false alarms and misses of snow depth for regularly measuring stations, at 30 h forecast range 22

3.15 Contingency tables showing percentage of accurate forecasts, false alarms and misses of snow depth for stations in different altitude groups, at 30 h forecast range 22
3.16 Map of excluded and used stations for measuring snow water equivalent, distinguishing 4 altitude categories 24
3.17 Weekly time series of snow water equivalent measurements and forecasts, averaged over all available-enough-stations, absolute bias and daily counts of available stations, at forecast ranges 6 and 30 hours 25
3.18 Time series of average weekly observed and forecast values of snow depth, forecast bias and counts of regularly measuring stations, at forecast ranges 6 and 30 hours 25
3.19 Scatter plots comparing forecast and observed snow water equivalent for different altitude groups, both axes with square root scale, at 6-hour forecast range 26
3.20 Time series of observed and forecast snow water equivalent averaged over all stations in upper altitudes, forecast bias and standard deviation, at 6 and 30-hour forecast ranges, barplots with counts of available stations 28
3.21 Time series of observed and forecast snow water equivalent averaged over all stations in mountain altitudes, forecast bias, 6 and 30-hour forecast ranges, barplots with counts of available stations 28
3.22 Frequency distribution of snow water equivalent forecast bias for stations in mountain altitudes, measurements comparable with snow depth, 6 h and 30 h forecast ranges 30
3.23 The same as in Fig. 3.22 for snow depth forecast 30
3.24 Time series of observed and forecast snow water equivalent averaged over all stations in low altitudes, forecast bias, 6 and 30-hour forecast ranges, barplots with counts of available stations 31
3.25 Weekly time series of used statistical scores for available enough, W_s-measuring stations in low altitudes, at 6 and 30 h forecast ranges 31
3.26 Weekly time series of used statistical scores for available enough, W_s-measuring stations in mountain altitudes, at 6 and 30 h forecast ranges 32
3.27 Contingency tables showing percentage of accurate forecasts, false alarms and misses of snow water equivalent forecast for regularly measuring stations, at 6 h forecast range 33
3.28 Contingency tables showing percentage of accurate forecasts, false alarms and misses of snow water equivalent forecast for stations in different altitude groups, at 6 h forecast range 33
3.29 Contingency tables showing percentage of accurate forecasts, false alarms and misses of snow water equivalent forecast for regularly measuring stations, at 30 h forecast range 34
3.30 Contingency tables showing percentage of accurate forecasts, false alarms and misses of snow water equivalent for stations in different altitude groups, at 30 h forecast range 34
3.31 Time series of observed and forecast density, absolute bias, barplots with counts of available stations, at 6 h forecast range 35

3.32 Histogram showing the distribution of observed density of snow . 36

List of Tables

3.1 Altitude limits of the 4 categories and percentage of Czechia's area covered by them 12
3.2 Counts of stations which measured snow depth at least once, counts of regularly measuring stations and their percentage of the original count 12
3.3 Values of used statistical characteristics for all regularly measuring (denoted rm) stations together and split accordingly to altitude groups, values of scores of all mountain stations measuring on Mondays, at 6 h forecast range 15
3.4 The same as in Tab. (3.3) for 30 h forecast range 16
3.5 Mean and standard deviation of bias distributions for all altitude groups, 6 h forecast range, zero bias values originating from correct forecast of no snow omitted, (regularly measuring stations denoted as rm) 19
3.6 The same as in Tab. 3.5 for 30 h forecast range 19
3.7 Counts of stations which measured snow water equivalent at least once, counts of stations measuring on at least 19 Mondays and their percentage of the original number of stations 23
3.8 Values of used statistical characteristics for all available enough (denoted avl) stations together and split accordingly to altitudes, at 6 h forecast range 27
3.9 The same as in Tab. 3.8 for 30 h forecast range 27
3.10 Mean and standard deviation of snow water equivalent forecast bias distributions for all altitude groups, at 6-hour forecast range, (avl denotes available enough stations) 29
3.11 The same as in Tab. 3.10 for 30 h forecast range 29

A.1 List of model constants and parameters used at CHMI 48
A.2 List of model variables used at CHMI 49

List of Abbreviations

ALADIN Aire Limitée, Adaptation Dynamique, Development InterNational - International development for limited-area dynamical adaptation

ALARO ALadin–AROme, where AROME stands for Application of Research to Operations at Mesoscale

ARPEGE Action de Recherche Petite Echelle Grande Echelle - Small-Scale Large-Scale Research Action

avl available enough stations

CHMI Czech HydroMeteorological Institute

CLIDATA Climatological Database Application used by CHMI

ISBA Interactions Sol Biosphère Atmosphère - Interactions between Biosphere and Atmosphere

rm regularly measuring stations

UTC Coordinated Universal Time

A. Attachments

A.1 Code implementation

In the code of ALADIN, snow parametrization is handled in three fortran subroutines called `ACSOL`, `CPTENDS` and `CPWTS`. In this section, only their key parts and correspondence with theoretical description will be shown. All relevant constant and parameter names together with their notation from the above equations are summarized in Tab. A.1. Similar information about used variables is in Tab. A.2.

A.1.1 Snow tendencies

Computation of snow tendencies is done by subroutine `CPTENDS`. The part of the this subroutine dealing with snow goes as follows:

```
1  IF ( LNEIGE ) THEN
2    DO JROF = KSTART, KPROF
3      PTDSNS(JROF) = PLSM(JROF) * ( PFPLCN(JROF,KFLEV) +&
4       & PFPLSN(JROF,KFLEV) - PFONTE(JROF)+PFEVN(JROF)-PFEVI(JROF))
5      IF (LSNV.OR.LVGSN) THEN
6        ZPRECN=PLSM(JROF)*(PFPLCN(JROF,KFLEV)+PFPLSN(JROF,KFLEV))
7        IF (PFONTE(JROF) > 0.0_JPRB) THEN
8          PTDALBNS(JROF) = -TOEXP*(PALBNS1(JROF)-ALBMIN)+ZPRECN/WNEW
9        ELSE
10         PTDALBNS(JROF) = -TOLIN+ZPRECN/WNEW
11       ENDIF
12       ZTO3 = MIN(0.5_JPRB/PDT,ZPRECN/MAX(PSNS1(JROF),ZEPSN))
13       PTDRHONS(JROF)= -TOEXP*(PRHONS1(JROF)-RHOMAX)&
14        & -ZTO3*(PRHONS1(JROF)-RHOMIN)
15     ENDIF
16   ENDDO
17 ENDIF
```

Here `LNEIGE` is a logical switch for usage of the snow scheme, `JROF` is a horizontal gridbox index and `KSTART` and `KPROF` are its boundaries. `KFLEV` then represents the lowest vertical model layer.

Taking into account Tab. A.2 and line 6, which defines the solid precipitation flux P_s as a sum of convective and stratiform snow fluxes, it can be seen that lines 3 and 4 deal with the computation of the tendecy of snow reservoir and are equivalent to Eq. (1.2). Lines 7-11 then serve for determining the tendency of snow albedo and stand for Eq. (1.4). Time tendency of snow density according to Eq. (1.6) is then covered by lines 12-14.

A.1.2 Snow variables evolution

The actual values of prognostic snow variables W_s, A_s and ρ_s are calculated in subroutine `CPWTS`:

```
1  IF ( LNEIGE ) THEN
2    DO JROF = KSTART,KPROF
3      PSNS1(JROF) = PSNS1(JROF) + PDT * PTDSNS(JROF)
4      IF (LSOLV) THEN
5      ...
```

```
6       PSNS1(JROF) = MAX(0.0_JPRB,PSNS1(JROF))
7       IF (LSNV.OR.LVGSN) THEN
8         IF (PSNS1(JROF) > 0.0_JPRB) THEN
9           PALBNS1(JROF) = PALBNS1(JROF)+PTDALBNS(JROF)*PDT
10          PALBNS1(JROF) = MIN(MAX(PALBNS1(JROF),ALBMIN),ALBMAX)
11        ELSE
12          PALBNS1(JROF) = ALBMAX
13        ENDIF
14        IF (PSNS1(JROF) > 0) THEN
15          PRHONS1(JROF) = PRHONS1(JROF)+PTDRHONS(JROF)*PDT
16          PRHONS1(JROF) = MIN(MAX(PRHONS1(JROF),RHOMIN),RHOMAX)
17        ELSE
18          PRHONS1(JROF) = RHOMIN
19        ENDIF
20      ENDIF
21    ENDDO
22  ENDIF
```

Here line 3 determines the value of snow reservoir W_s from its time tendency $\frac{\partial W_s}{\partial t}$ as is written in Eq. (1.1). Line 6 ensures a non-negative value of snow reservoir accordingly to Eq. (1.3).

The values of snow albedo and snow density computed according to Eq. (1.1) are calculated on lines 9 and 15 respectively. The physical limitations given by Eq. (1.5) and Eq. (1.8) are then secured by lines 10 and 16. In case of no snow reservoir when `PSNS1` $= 0$, snow albedo is set to its maximum, while snow density to its minimum value. That makes the variables ready for snowfall, since maximum albedo and minimum density are the characteristics of fresh snow.

A.1.3 Snow fractions

Snow fractions are calculated by subroutine `ACSOL`. The part of the code valid for the Bazile et al. [2001] scheme is

```
1  ZUZ0CN = 1.0_JPRB/(RG*ALRCN2)
2  ELSEIF (LVGSN) THEN
3    IF (LZ0HSREL.AND.LCOEFKSURF) THEN
4      PNEIJG(JLON)=PLSM(JLON)*PSNS(JLON)/(PSNS(JLON)+WCRIN* &
5        & (1.0_JPRB+ZUZ0CN*PGZ0HF(JLON)/STHER))
6    ELSE
7      PNEIJG(JLON)=PLSM(JLON)*PSNS(JLON)/(PSNS(JLON)+WCRIN)
8    ENDIF
9    ZCFN =(1.0_JPRB-MAX(0.0_JPRB,MIN(1.0_JPRB,PLAI(JLON)/RLAIMX)))* &
10     & MAX(0.0_JPRB,SIGN(1.0_JPRB,PLAI(JLON)-RLAI))+ &
11     & (1.0_JPRB-MAX(0.0_JPRB,SIGN(1.0_JPRB,PLAI(JLON)-RLAI)))
12   ZCK = MAX(0.0_JPRB,(ALB1-MAX(ALB2,PALBNS(JLON))))/(ALB1-ALB2)
13   ZCOEF=ZCFN*ZCK+(1.0_JPRB-ZCK)
14   PNEIJV(JLON)=PNEIJG(JLON)*ZCOEF
15 ENDIF
```

According to Mašek [2018], the option `LZOHSREL` specifies the way of determining thermal roughness. Thermal roughness z_{0H} is an analogue of mechanical roughness length, applied on heat and moisture turbulent transfers (Ridgen et al. [2017]). In case of `LZOHSREL` $=$ F, which corresponds to line 6, effective thermal roughness is determined as

$$z_{0H}^{eff} = s_{ther}\sqrt{(z_{0D})^2 + (z_{0D}^{orog})^2},$$

where z_{0D} stands for dynamic roughness caused by micrometeorological objects such as vegetation and rocks, while z_{0D}^{orog} takes into account the subgrid variations of terrain elevation. Here s_{ther} denotes the ratio of thermal to dynamic roughness which is for ISBA approximated by a constant $s_{ther} = 0.1$. However, for this setting of `LZOHSREL`, surface roughness is not used for any quantity concerning snow at all and snow fraction is estimated on line 7 simply as

$$f_s^{bg} = \frac{W_s}{W_s + W_s^{crit}}.$$

For the setting `LZOHSREL` = T which is used on line 3, and which is currently being used at CHMI, thermal roughness does not have an orographic component, which is in better agreement with theory (Hewer and Wood [1998]). In other words

$$z_{0H} = s_{ther} z_{0D}. \tag{A.1}$$

Using notation from Tab. A.1 and Tab. A.2 and plugging in for `ZUZOCN` from line 1, lines 4 and 5 can be rewritten in symbolic form as

$$f_s^{bg} = \frac{W_s}{W_s + W_s^{crit}(1 + \frac{z_{0H}^{bg}}{a_2 \cdot s_{ther}})},$$

from which, considering Eq. (A.1), it can be seen that these lines are equivalent to Eq. (1.10).

On line 13 the above-mentioned function $F(LAI, A_s) \equiv$ `ZCOEF` is computed from variables `ZCFN` and `ZCK`. The `SIGN` functions on lines 10 and 11 acquire a negative value in case of $LAI < 3 \equiv$ `RLAI` and cause the associated maximum functions to become 0. That results in `ZCFN` = 1 which leads to `ZCOEF` being 1 regardless of the value of `ZCK`, which is consistent with Eq. (1.11).

In case of $LAI \geq 3$

$$\texttt{ZCFN} = \min\Big(1 - \frac{LAI}{K_{lai}}, 1\Big).$$

However, for the values of albedo constants in Tab. A.1 it holds, that the maximum function in `ZCK` can be omitted and

$$\texttt{ZCK} = \frac{A_1 - max(A_2, A_s)}{A_1 - A_0},$$

from which it can be derived, that variable $F(LAI, A_s) = \texttt{ZCFN} \cdot \texttt{ZCK} + (1 - \texttt{ZCK})$ takes on the form mentioned in Eq. (1.11).

Table A.1: List of model constants and parameters used at CHMI

code variable	eq. notation	value	unit
ZEPSN	ϵ	10^{-3}	[1]
TOEXP	r_{exp}	$\frac{0.24}{86400}$	[1/s]
TOLIN	r_{lin}	$\frac{0.008}{86400}$	[1/s]
ALBMIN	A_s^{min}	0.5	[1]
ALBMAX	A_s^{max}	0.85	[1]
RHOMIN	ρ_s^{min}	0.1	$[g\,cm^{-3}]$
RHOMAX	ρ_s^{max}	0.3	$[g\,cm^{-3}]$
WNEW	W_s^{new}	10	$[kg\,m^{-2}]$
WCRIN	W_s^{crit}	4	$[kg\,m^{-2}]$
RG	g	9.80665	$[m\,s^{-2}]$
STHER	s_{ther}	0.1	[1]
ALRCN2	a_2	10	[1]
ALB1	A_1	0.87	[1]
ALB2	A_2	0.84	[1]
RLAIMX	K_{lai}	7	[1]
RLAI		3	[1]

Table A.2: List of model variables used at CHMI

code variable	eq. notation	unit	meaning
PSNS	W_s	$[kg\,m^{-2}]$	snow reservoir
ZPRECN	P_s	$[kg\,m^{-2}\,s^{-1}]$	solid precipitation flux
PFONTE	F_m	$[kg\,m^{-2}\,s^{-1}]$	snow melting flux
PFEVN	F_{evs}	$[kg\,m^{-2}\,s^{-1}]$	evaporation flux of solid reservoirs
PFEVI	F_{evi}	$[kg\,m^{-2}\,s^{-1}]$	evaporation flux from ice
PALBSN1	A_s	[1]	snow albedo
PRHONS1	ρ_s	$[g\,cm^{-3}]$	snow density
PTDSNS	$\frac{\partial W_s}{\partial t}$	$[kg\,m^{-2}\,s^{-1}]$	tendency of snow reservoir
PTDALBNS	$\frac{\partial A_s}{\partial t}$	$[s^{-1}]$	tendency of snow albedo
PTDRHONS	$\frac{\partial \rho_s}{\partial t}$	$[g\,cm^{-3}\,s^{-1}]$	tendency of snow density
PNEIG	f_s^{bg}	[1]	snow fraction over bare ground
PGZ0HF	$g\,z_{0H}^{bg}$	$[J\,kg^{-1}]$	Earth's gravity · thermal roughness
PDT	Δt	$[s]$	integration timestep
ZCOF	$F(LAI, A_s)$	[1]	reduction of f_s on vegetation
PFPLCN		$[kg\,m^{-2}\,s^{-1}]$	prec. flux of convective snow
PFPLSN		$[kg\,m^{-2}\,s^{-1}]$	prec. flux of stratiform snow
PLSM			land sea binary mask
PIVEG			vegetation index